Redox Biology 67 (2023) 102915

Contents lists available at ScienceDirect

Redox Biology

journal homepage: www.elsevier.com/locate/redox

Clozapine suppresses NADPH oxidase activation, counteracts cytosolic H_2O_2, and triggers early onset mitochondrial dysfunction during adipogenesis of human liposarcoma SW872 cells

Giulia Blandino [a,1], Mara Fiorani [a,*,1], Barbara Canonico [a], Rita De Matteis [a], Andrea Guidarelli [a], Mariele Montanari [a], Gloria Buffi [a], Lucia Coppo [b], Elias S.J. Arnér [b,c], Orazio Cantoni [a]

[a] Department of Biomolecular Sciences, University of Urbino Carlo Bo, Urbino, Italy
[b] Division of Biochemistry, Department of Medical Biochemistry and Biophysics, Karolinska Institutet, Stockholm, Sweden
[c] Department of Selenoprotein Research and the National Tumor Biology Laboratory, National Institute of Oncology, Budapest, Hungary

ARTICLE INFO

Keywords:
Adipocyte differentiation
Clozapine
NADPH oxidase
Mitochondrial ROS
Mitochondrial dysfunction

ABSTRACT

Long-term treatment of schizophrenia with clozapine (CLZ), an atypical antipsychotic drug, is associated with an increased incidence of metabolic disorders mediated by poorly understood mechanisms. We herein report that CLZ, while slowing down the morphological changes and lipid accumulation occurring during SW872 cell adipogenesis, also causes an early (day 3) inhibition of the expression/nuclear translocation of CAAT/enhancer-binding protein β and peroxisome proliferator-activated receptor γ. Under the same conditions, CLZ blunts NADPH oxidase-derived reactive oxygen species (ROS) by a dual mechanism involving enzyme inhibition and ROS scavenging. These effects were accompanied by hampered activation of the nuclear factor (erythroid-derived2)-like 2 (Nrf2)-dependent antioxidant responses compared to controls, and by an aggravated formation of mitochondrial superoxide. CLZ failed to exert ROS scavenging activities in the mitochondrial compartment but appeared to actively scavenge cytosolic H_2O_2 derived from mitochondrial superoxide. The early formation of mitochondrial ROS promoted by CLZ was also associated with signs of mitochondrial dysfunction. Some of the above findings were recapitulated using mouse embryonic fibroblasts.

We conclude that the NADPH oxidase inhibitory and cytosolic ROS scavenging activities of CLZ slow down SW872 cell adipogenesis and suppress their Nrf2 activation, an event apparently connected with increased mitochondrial ROS formation, which is associated with insulin resistance and metabolic syndrome. Thus, the cellular events characterised herein may help to shed light on the more detailed molecular mechanisms explaining some of the adverse metabolic effects of CLZ.

1. Introduction

Second generation antipsychotics (SGAs) are fundamental drugs for the cure of schizophrenia and other psychiatric disorders. SGAs present important advantages with respect to first-generation antipsychotics, as they effectively control both the positive and negative symptoms of schizophrenia, with a significant reduction of extrapyramidal side effects. However, SGAs are not immune from severe reactions. Indeed, substantial evidence links SGA exposure to metabolic impairment, making patients more vulnerable to cardiovascular alterations, hypertension, hyperlipidaemia, body weight gain, insulin resistance and type 2 diabetes [1–4].

Clozapine (CLZ) is one of the most effective SGAs, frequently employed to treat psychosis resistant to other pharmacotherapies [5] and severely ill patients [6], which however also causes serious cardiovascular complications [7,8] and body weight gain [9,10].

The identification of the mechanism(s) mediating the metabolic effects of CLZ is complicated by the complexity of its pharmacological profile, characterised by antagonism to various subtypes of dopaminergic, serotoninergic, noradrenergic, muscarinic, and histaminergic receptors [10–12], as well as by other receptor-independent effects [13,14]. Indeed, CLZ inhibits the activity of enzymes such as pyruvate kinase, mitochondrial malate dehydrogenase, succinate dehydrogenase

* Corresponding author. Department of Biomolecular Sciences, University of Urbino Carlo Bo, Via Saffi 2 61029 Urbino, PU, Italy.
E-mail address: mara.fiorani@uniurb.it (M. Fiorani).
[1] These authors contributed equally.

https://doi.org/10.1016/j.redox.2023.102915
Received 21 July 2023; Received in revised form 29 September 2023; Accepted 1 October 2023
Available online 12 October 2023

Abbreviations

C/EBPs	CAAT/enhancer-binding proteins
CLZ	clozapine
DCF	chloromethyl-2′,7′-dichlorodihydrofluorescein diacetate
DM	differentiation medium
DTNB	dithiobis-2-nitrobenzoic acid
GCL	glutamate-cysteine ligase
Glut4	Glucose Transporter Type 4
HPLC	high performance liquid chromatography
IBMX	3-isobutyl-1-methylxanthine
LD	lipid droplet
MEF	mouse embryonic fibroblast
NAO	nonyl acridine orange
NOX-2	NADPH oxidase-2
NQO1	NAD(P)H: quinone oxidoreductase 1
NR	Nile Red
Nrf2	nuclear factor (erythroid-derived2)-like 2
ORO	Oil Red O
PMA	phorbol-12-myristate-13-acetate
PPARγ	peroxisome proliferator-activated receptor γ
qPCR	quantitative real time PCR
ROS	reactive oxygen species
SDS	sodium dodecyl sulphate
SGAs	second generation antipsychotics
TrxR-1	thioredoxin reductase-1
Trx-1	thioredoxin-1
Trx-2	thioredoxin-2

and cytochrome oxidase [15–17] and causes other effects which may potentially contribute to the induction of mitochondrial dysfunction [18], an event implicated in insulin resistance and more generally in metabolic syndrome [19,20]. As a final note, CLZ has been reported to induce mitochondrial dysfunction in cell types of different origin, through yet undefined mechanisms [18].

Although mitochondrial dysfunction is often associated with the formation of reactive oxygen species (ROS), CLZ can also counteract oxidative stress, for example through inhibition of NADPH oxidase-2 (NOX-2) [21,22] or by having a direct antioxidant activity [23–25]. The lipophilic nature of CLZ is critical to determine its final concentration in different cellular compartments and tissues. The sub-cellular compartmentalization of the drug should also represent a critical determinant of the redox signalling pathways affected. These important characteristics of CLZ have potential implications in numerous processes regulated by ROS, which also include adipogenesis [26–28].

Based on the above considerations, studies using cultured cells have attempted to address the issues of the direct effects of CLZ in processes associated with the conversion of pre-adipocytes to mature adipocytes, demonstrating that the SGA up-regulates fat-specific markers [29] and stimulates adipogenesis in murine 3T3L1 cells [30–32]. In a recent study, we characterised the differentiation process of human liposarcoma SW872 cells and identified an early formation of NOX-2 derived ROS, apparently associated with critical biochemical events regulating the conversion of pre-adipocytes to mature adipocytes [33]. This early phase was followed by a late phase instead characterised by the emission of mitochondrial ROS and by the onset of mitochondrial dysfunction.

Here we reasoned that the antioxidant and NOX-2 inhibitory properties of CLZ might impact on the early ROS signalling of differentiating SW872 cells, thereby affecting an array of downstream events during the adipogenic process. We report results consistent with this notion, establishing a link between these effects and a delay of the progression of adipogenesis. Most importantly, however, suppression of early ROS formation was associated with the inhibition of nuclear factor (erythroid-derived2)-like 2 (Nrf2)-dependent activation of antioxidant defense that was seen in control cells. Consequently, CLZ, apparently failing to induce ROS scavenging in the mitochondrial compartment, promoted an early formation of mitochondrial ROS and mitochondrial dysfunction.

2. Materials and methods

2.1. Materials

Acrylamide 30 %, glycine, sodium dodecyl sulphate (SDS), methanol, acetonitrile, insulin, dexamethasone, 3-isobutyl-1-methylxanthine (IBMX), DL-Dithiothreitol (DTT), oleic acid-albumin and linoleic acid-albumin, Oil Red O (ORO), Glutathione (GSH), dithiobis-2-nitrobenzoic acid (DTNB), TWEEN 20, isopropanol, glacial *meta*-phosphoric acid as well most of the reagent-grade chemicals were purchased from Merck Life Science s.r.l. (Milan, Italy). Auranofin, Sodium arsenite, ATP, phorbol-12-myristate-13-acetate (PMA), catalase, H_2O_2 were purchased from Sigma-Aldrich (Milan, Italy). Glycerol, Sodium chloride, EDTA, Na_2HPO_4, KH_2PO_4 and K_2HPO_4 were from Carlo Erba (Milan, Italy). HRP was from SERVA. Luminol was from Alfa Aesar. NADPH tetrasodium salt was purchased from Saaven Werner. WesternBright™ ECL (K-12045-D20) was from Advansta-Aurogenes s.r.l (Rome, Italy). Clarity Max was from Biorad Laboratories s.r.l. (Milan, Italy). CLZ (S2459) was purchased from Selleckchem (Planegg, Germany).

2.2. Cell culture conditions

Human liposarcoma SW872 cells were purchased from the American Type Culture Collection (Rockville, Maryland, USA) and used between passages 3 and 14. Cells were maintained in Dulbecco's modified Eagle medium/nutrient mixture F-12 (DMEM/F12) Merck Life Science s.r.l., supplemented with 10 % foetal bovine serum (FBS) (35-079-CV, Corning-S.I.A.L. s.r.l, Rome, Italy), 100 U/ml penicillin and 100 μg/ml streptomycin. U937 human myeloid leukaemia cells were cultured in suspension in RPMI 1640 medium (Sigma Aldrich) supplemented with 10 % FBS, 100 U/ml penicillin and 100 μg/ml streptomycin. Post-confluent SW872 were induced to adipogenic differentiation by changing the regular growth medium to differentiation medium (DM), containing several differentiation factors including hormonal inducers such as dexamethasone and insulin, as described previously [33].

Primary mouse embryonic fibroblasts (MEFs) [34] were kindly provided by Prof Ester Zito (Istituto di Ricerche Farmacologiche Mario Negri IRCCS, Milan, Italy) and cultured in DMEM - high glucose (6546, Merck Life Science s.r.l.) supplemented with 2 mM L-glutamine (Euroclone), 100 U/ml penicillin, 100 μg/ml streptomycin and 10 % FBS. Post-confluent MEFs were induced to differentiate in a DM containing 0.5 mM IBMX, 830 nM insulin and 1 μM dexamethasone.

CLZ stock solution was prepared in dimethyl sulfoxide (DMSO) at a concentration of 10 mM. The final DMSO concentration never exceeded 0.15 %. CLZ was added to the DM at the concentrations reported in the legends to the figures and the same procedure was repeated after 48 h. Controls (CTR) received DMSO alone.

2.3. Oil Red O staining

SW872 cell neutral lipids were visualized using the soluble selective dye ORO, as described in Ref. [33]. Briefly, cells were washed with potassium phosphate-buffered saline (PBS: 136 mM NaCl, 10 mM Na_2HPO_4, 1.5 mM KH_2PO_4, 3 mM KCl; pH 7.4), fixed with 4 % formaldehyde in PBS (1 h, room temperature, RT), washed with PBS, and

incubated with isopropanol 60 % (1 min, RT). Then, samples were stained with 0.3 % ORO working solution (1 h, RT). The ORO working solution was freshly prepared and filtered before use. After several washes with PBS, lipid droplet formation was followed on an inverted microscope (Axio Vert.A1, Carl Zeiss, Germany) equipped with a Canon EOS 1100 D camera. Cellular ORO quantification was performed by eluting the dye with 100 % isopropanol and measuring the absorption at 510 nm.

ORO staining was performed in MEFs on glass slides, processed as described in Ref. [33]. The slides were incubated with the ORO working solution for 1 h at RT, washed twice with H_2O, counterstained with hematoxylin to visualize nuclei, and mounted in glycerol gel (Sigma-Aldrich-SIAL Rome, Italy).

2.4. Enzyme activities

Thioredoxin Reductase-1 (TrxR-1) activity was determined with the Thioredoxin (Trx) dependent insulin reduction assay, as described in Ref. [35]. Recombinant Trx and TrxR proteins were produced as described previously [36]. In short, total cell lysate protein was incubated with 0.275 mM human insulin, 1.3 mM NADPH and 20 μM human Trx for 30 min in 96-well plates at 37 °C in TE buffer (50 mM Tris-HCl, 2 mM EDTA, pH 7.5) [36]. Finally, a mixture of 6 M guanidine HCl and 1 mM DTNB was added to the plates and the absorbance at 412 nm was measured using a microplate spectrophotometer (TECAN Infinite M200 Pro). To measure Trx-1 activity, samples were incubated with the above-described mix, but replacing Trx-1 with 20 nM TrxR-1. The absorbance values were normalized by the protein concentrations measured using Pierce bicinchoninic acid assay protein assay kit (Thermo Fischer Scientific) according to the manufacturer's protocol.

2.5. RNA extraction and cDNA synthesis

Total RNA extraction was performed with the miRNeasy Mini Kit (Qiagen, Hilden, Germany) after direct lysis with 700 μl of QIAzol Lysis Reagent (Qiagen, Hilden, Germany). Extracted RNA was quantified with a Micro UV–Vis Spectrophotometer Nanoready (Life Real, Hangzhou, Zhejiang, China). Total RNA (500 ng) was reverse transcribed using PrimeScriptTM RT Master Mix (Perfect Real Time) (Takara Bio Inc.) according to the manufacturer instructions with a GeneExplorer Thermal Cycler (Hangzhou Bioer Technology Co., Ltd).

2.6. Quantitative real-time PCR (qPCR)

The gene expression was evaluated by qPCR as previously described [37]. Briefly, the qPCR reactions were carried out in duplicate in a final volume of 20 μl using TB Green PreMix ex Taq II Master Mix (Takara Bio Europe, France) and 200 nM primers listed in Fig. S10 in a RotorGene 6000 instrument (Corbett life science, Sydney, Australia). The amplification conditions were: 95 °C for 10 min, 40 cycles at 95 °C for 10 s and 60 °C for 50 s, followed by a melting curve analysis at the end of each run from 65 to 95 °C, to exclude the presence of non-specific products or primer dimers. A duplicate non-template control was included for each primer pair reaction as negative control. The relative expression levels were calculated by the $2^{-\Delta\Delta Ct}$ method [38] using GAPDH or HPRT as reference genes for SW872 cells or MEFs, respectively.

2.7. Western Blot

Western Blot analysis were performed as described in Ref. [33]. Briefly, cell lysate proteins (25/35 μg) were separated by SDS poly-acrylamide gel electrophoresis and then probed with anti-CAAT/enhancer-binding protein β (C/EBPβ) (1:1000; sc-150; Santa Cruz Biotech, Santa Cruz CA), anti-peroxisome proliferator-activated receptor γ (PPARγ) (1:1000; 81B8; Cell Signalling, USA), anti-Nrf2 (1:1000; D1Z9C; Cell Signalling, USA), anti- NAD(P)H:quinone oxidoreductase 1 (NQO1) (1:1000; A180; Cell Signalling, USA), anti-Trx-1 (1:1000; ATRX-03; IMCO Ltd), anti-GAPDH (1:1000; sc-47724, Santa Cruz Biotech, Santa Cruz CA), anti-Actin (1:1000; VMA00048, Biorad), anti-TrxR-1 (1:1000; sc-58444; Santa Cruz Biotech, Santa Cruz CA), anti-Trx-2 (1:1000; sc-133201; Santa Cruz Biotech, Santa Cruz CA) at 4 °C overnight. After washing 3 times with TBS-T, membranes were further probed with goat anti-rabbit IgG-HRP (1:5000; sc-2004; Santa Cruz Biotech, Santa Cruz CA), with m-IgGk BP-HRP (1:5000; sc-516102; Santa Cruz Biotech) or with rabbit anti-goat IgG (H + L)-HRP (1:5000; 6160-05; SouthernBiotech; UK) for 2 h at RT. Bands were detected using the chemiluminescence system (WesternBright™ ECL). The density of the corresponding bands was measured quantitatively using National Institutes of Health (NIH) Image software (http://rsb.info.nih.gov/nih-image). In Fig. S11 the uncut Western blot membranes are reported. Validation of Trx-1, TrxR-1 and NQO1, Nrf2 and Keap1 WB analyses by using KO cells was reported in Fig. S12.

2.8. Evaluation of DNA content and sub diploid peak by flow cytometry

Cells were harvested and fixed with 70 % cold (−20 °C) ethanol. Samples were washed twice with PBS and pellets were resuspended in PBS, containing 20 μg/ml propidium iodide (PI) and 100 μg/ml RNAse. Samples were kept at 37 °C in the dark for at least 30 min and analysed for cell cycle profile by means of a FACSCanto™ flow cytometer equipped with three lasers. Data were acquired and analysed by FACS-Diva™ flow cytometry software (Becton Dickinson, San Jose, CA).

2.9. Measurement of GSH content

Cellular GSH was measured by high performance liquid chromatography (HPLC) as described in Ref. [39]. Briefly, the cellular pellet was suspended in lysis buffer (0.1 % Triton X-100; 0.1 M Na_2HPO_4; 5 mM Na-EDTA, pH 7.5), vortexed and kept for 10 min on ice. Thereafter, 0.1 N HCl and the precipitating solution (0.2 M glacial *meta*-phosphoric acid, 5 mM sodium EDTA, 0.5 M NaCl) were added to the samples. After centrifugation, the supernatants were collected and kept at −80 °C until HPLC analyses. Just before analysis, DTNB (20 mg in 100 ml of 1 % w/v sodium citrate) was added to the extracts. The samples were filtered through 0.22 μm pore micro-filters and finally analysed for their GSH content by HPLC, using a 15 cm × 4.6 mm, 5 μm Supelco Discovery® C18 column (Supelco, Bellefonte, PA). The UV absorption was detected at 330 nm. The injection volume was 20 μl. The retention time of GSH was approximately 15.7 min.

2.10. BODIPY 493/503 staining of neutral lipid droplets for microscopy

After treatments, MEFs were incubated with 2 μM 4,4-difluoro-1,3,5,7,8-pentamethyl-4-bora-3a,4a-diaza-s-indacene (BODIPY 493/503) in medium with 0.25 % FBS in a cell culture incubator for 20 min. Cells were washed twice with PBS and fixed with 4 % formalin for 30 min at RT. Finally, images were visualized using a fluorescence microscope and the fluorescence intensity was quantified by ImageJ software [40].

2.11. Redox Western Blot

The mitochondrial Trx-2 redox state, having only one active site dithiol-disulfide motif without additional Cys residues, was measured by a redox Western blot approach as described by Guidarelli et al. [41]. Briefly, cells were washed with PBS and detached from the culture dish in 200 μl urea lysis buffer (100 mM Tris/HCl, pH 8.2; urea 8 M; EDTA 1 mM) containing 10 mM iodoacetamide. The samples were then incubated for 20 min at 37 °C and centrifuged for 1 min at 14,000g. Ten volumes of cold acetone/1 M HCl (98:2) were added to the supernatants and the pellets were washed twice with acetone/1 M HCl/H_2O (98.2:10). The pellets were resuspended in 80 μl of urea lysis buffer

containing 3.5 mM dithiothreitol and after 30 min incubation at 37 °C, samples were incubated for a further 30 min at the same temperature in the presence of 30 mM iodoacetic acid. Samples were then subjected to urea polyacrylamide gel electrophoresis (7 M urea and 7 % acrylamide), under non reducing conditions, and blotted [42]. In Fig. S11 the uncut Western blot membranes are reported.

2.12. Flow cytometric staining of fresh, unfixed cells for pan ROS detection

Cells were labelled with MitoSOX red (5 μM, 10 min) (Thermo Fisher Scientific, Milan, Italy), a dye targeting the mitochondria of live cells, selectively oxidized by $O_2^{\cdot-}$ to produce red fluorescence [43]. Chloromethyl-2′,7′-dichlorodihydrofluorescein diacetate (DCF, 5 μM, 30 min) (Thermo Fisher Scientific), a general probe for ROS detection [44], was also used. The cardiolipin-sensitive probe 10-nonyl acridine orange (NAO) (Molecular Probes, Leiden, The Netherlands) was applied (15 min) at a final concentration of 100 nM, as indicated in Ref. [33].

2.13. Flow cytometric and confocal staining of fixed/permeabilised cells for NADPH oxidase subunits

SW872 cells were washed with PBS at RT and resuspended in 100 μl of Dako Intrastain Reagent A (Dako, Agilent, Santa Clara, CA). After 15 min of incubation, cells were washed and resuspended in 100 μl of Dako Intrastain Reagent B [45]. Anti-phosphorylated $p47^{phox}$ (STJ91180; St. John's Laboratory, UK), anti-$p67^{phox}$ (CQA1036; Cohesion Biosciences) and anti-$p47^{phox}$ (SAB4502810; Merck Life Science s.r.l) were incubated for 30 min at 4 °C; after a washing step, anti-rabbit IgG-FITC antibody was added (sc-2012; Santa Cruz Biotech, Santa Cruz CA), as indicated in the manufacturer's instructions. Finally, cells were incubated for 30 min at 4 °C before being processed for flow cytometric and/or confocal microscopy analysis. All cytometric experiments were carried out with a FACSCanto II flow cytometer (BD, Franklin, Lakes, NJ, USA) equipped with an argon laser (Blue, Excitation 488 nm), a helium-neon laser (Red, Excitation 633 nm), and a solid-state diode laser (Violet, Ex 405 nm). Analyses were performed with the FACSDiva™ software (BD); approximately 10,000 cell events were acquired for each sample. Negative controls for phosphorilated-$p47^{phox}$ were performed by in-parallel omission of the secondary antibody, as reported in Fig. S13.

2.14. Flow cytometric staining with Nile red (NR)

MEFs were labelled for 15 min with 1 μg/ml NR (1000X stock solution was dissolved in DMSO), as reported in Fiorani et al., 2021 [33]. At least 10,000 events were acquired for each sample.

2.15. Morphology of mitochondrial network by confocal analyses

To evaluate the mitochondrial morphology, the cells were grown on MatTek glass bottom chambers (MatTek Corporation) and stained with MitoTracker Deep red 50 nM (Molecular Probes, Leiden, The Netherlands) for 20 min at 37 °C in 5 % CO_2. Confocal microscopy analyses were performed with a Leica TCS SP5 II confocal microscope (Leica Microsystem, Germany), with 488, 543, and 633 nm illuminations and oil-immersed objectives. The images were further processed and analysed in ImageJ software (NIH, Bethesda, MD, USA).

2.16. Immunocytochemistry

Cells grown on microslides were fixed with 4 % formaldehyde in PBS (15 min), washed twice with PBS and eventually permeabilized (10 min) with PBS containing 0.25 % Triton-X 100. After fixation and permeabilization, cells were blocked with 2 % normal serum for 20 min at room temperature.

Immunostaining was carried out with anti-Nrf2, anti-C/EBPβ, anti-PPARγ. The immunoreaction was revealed with the avidin–biotin–peroxidase complex (ABC) method (Vector, Burlingame, CA, United States). Peroxidase activity was revealed by diaminobenzidine hydrochloride as chromogen (Sigma-Aldrich, SIAL, Rome, Italy). Nuclei were counterstained with hematoxylin (VWR International, Milan, Italy) and mounted in Eukitt (Kindler, Freiburg, Germany). Antibody specificities were tested by in-parallel omission of the primary antibodies in the immunocytochemical staining (Fig. S14). Preparations were examined using a Nikon light microscope (Nikon Eclipse 80i microscope, Laboratory Imaging, Czech Republic) and an ACT-2U image analyser linked to a Sony equipped with digital camera.

2.17. Single cell DCF and MitoSOX-red fluorescence assays

Logarithmically growing U937, SW872 and MEFs were seeded in 35 mm tissue culture dishes. After CLZ exposure, the cells were incubated for 30 min with either 5 μM DCF or 5 μM MitoSOX red, washed twice with PBS, and finally treated with PMA, H_2O_2, or ATP/arsenite. After treatments, the cells were washed with PBS three times and the fluorescence images were visualized using a fluorescence microscope. The excitation and emission wavelengths were 488 and 515 nm (DCF) and 510 and 580 nm (MitoSOX red), with a 5-nm slit width for both emission and excitation. Images were collected with exposure times of 100–400 ms, digitally acquired and processed for fluorescence determination at the single cell level by ImageJ software. Mean fluorescence values were determined by averaging the fluorescence values of at least 50 cells/treatment condition/experiment.

2.18. Statistical analysis

Data are expressed as mean ± SEM. Statistical differences were analysed by unpaired *t*-test and one-way ANOVA followed by Dunnett's test for multiple comparison using Prism 6.01 software (GraphPad Software). A value of $p < 0.05$ was considered significant.

3. Results

3.1. Clozapine slows down SW872 cell adipogenesis

Post-confluent SW872 cells, characterised by a fibroblast like shape and the virtual absence of lipid droplets (LDs) (time zero sample, T0), undergo progressive changes in morphology when grown in DM for ten days (Fig. 1A). Under the same conditions, cells accumulate significant amounts of lipids in the forms of LDs, as it can be well appreciated by visual inspection of the cultures stained with ORO (Fig. 1A) and after ORO quantification (Fig. 1B). We investigated the effect of CLZ supplementation at the time of DM addition on lipid accumulation, and for this purpose employed concentrations of the SGA ≤ than 15 μM. These concentrations are slightly higher than those found in the bloodstream of treated patients [46–48] but are probably in the right range if one considers the accumulation of this lipophilic drug in the adipose tissue. Furthermore, these concentrations are much lower than those utilised in other studies [15,18,49,50].

As illustrated in Fig. 1A and B, addition of 15 μM CLZ at the time of DM supplementation significantly reduced the rate of lipid accumulation over the 10 days of growth. We decided to focus on the effects mediated by the SGA at the early times of differentiation, in which we previously detected significant redox changes [33]. We therefore performed our experiments at T3 and determined that the inhibitory effects of the drug on LD accumulation were concentration-dependent over a 5–15 μM concentration range (Fig. S1A). In addition, at this time point, flow cytometric analysis failed to reveal sub-diploid peaks in cells which did or did not receive 15 μM CLZ (Fig. S1B). Furthermore, the above inhibitory effects are detected under nontoxic conditions (Fig. S1C). Most of the experiments described below were therefore performed using 15 μM CLZ.

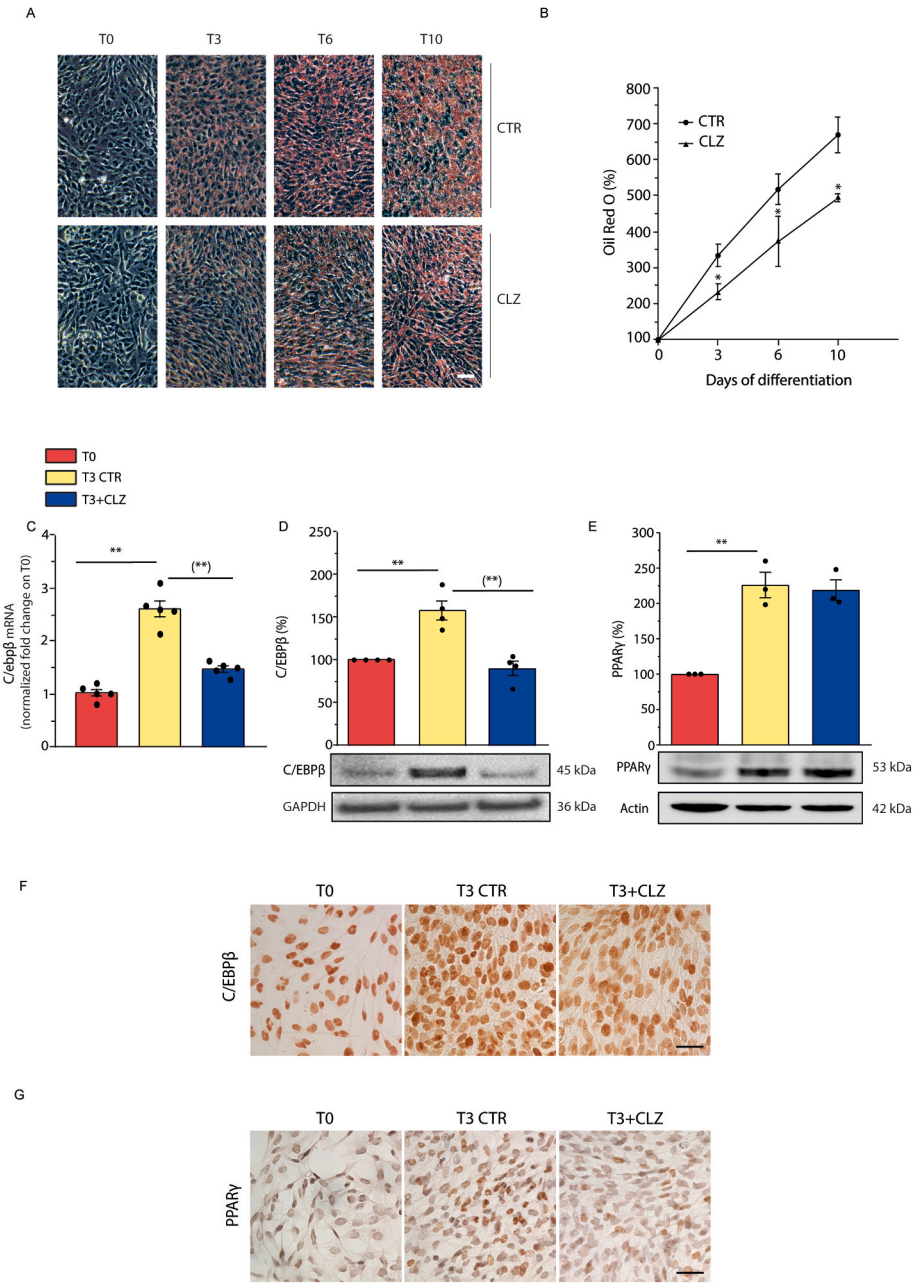

Fig. 1. Clozapine slows down the morphological and biochemical changes occurring during differentiation of SW872 cells.
(A) Representative images of ORO-stained LDs in differentiating SW872 cells grown for 10 days with or without CLZ (15 μM). Magnification 20X; scale bar represents 100 μm. (B) ORO quantification by spectrophotometric analysis at 510 nm. CTR samples received DMSO alone. Data are expressed in % respect to T0 condition. Results represent the means ± SEM calculated from at least three independent determinations, *$p < 0.05$, as compared to the CTR samples (Unpaired *t*-test). (C) Quantitative real time PCR of C/EBPβ expression after 3 days of differentiation (T3) with or without CLZ. The graph shows the normalized fold change compared to T0. GAPDH was used as housekeeping. (D) Western immunoblotting analysis of C/EBPβ. GAPDH was used as loading control. (E) Western immunoblotting analysis of PPARγ. Actin was used as loading control. T3 CTR received DMSO alone. Data are expressed in % respect to T0. Results represent the means ± SEM calculated from at least three independent determinations. **$p < 0.01$, as compared to T0; (**)$p < 0.01$, as compared to T3 (one-way ANOVA followed by Dunnett's test). (F–G) Immunocytochemical analysis of C/EBPβ and PPARγ expression at T3 with or without CLZ (Magnification 40X; scale bar represents 40 μm). Immunolocalization was visualized using diaminobenzidine (brown). Nuclei were counterstained with hematoxylin (blue grey). (For interpretation of the references to colour in this figure legend, the reader is referred to the Web version of this article.)

We found that expression of C/EBPβ, a master regulator of adipogenesis [51], detected at T3 at both the mRNA (Fig. 1C) and protein (Fig. 1D) levels, was abolished by CLZ. Consistently, under the same conditions, immunocytochemical analyses (Fig. 1F) provided evidence for increased nuclear C/EBPβ-immunostaining also sensitive to CLZ.

The effects were less prominent with PPARγ, another critical regulator of adipogenesis [52,53], since its increased expression, clearly detected at T3, was not affected by CLZ (Fig. 1E). However, the SGA inhibited the translocation of PPARγ to the nuclear compartment (Fig. 1G). The percentage of PPARγ immunoreactive (i.r.) nuclei at T0 corresponded to 13.2 ± 2.4. This percentage remarkably increased at T3 (44.5 ± 5.4; $p < 0.01$) and CLZ significantly reduced this response (27.9 ± 2.4; $p < 0.01$).

The results presented here show that CLZ slows down lipid accumulation in differentiating SW872 cells and under the same conditions inhibits C/EBPβ and PPARγ expression and/or nuclear translocation. We

next addressed whether these effects of CLZ were redox related.

3.2. Clozapine suppresses early ROS formation and NOX-2 activation

We have previously found that differentiating SW872 cells display an early ROS formation, at least in part attributable to NOX-2 activation [33]. By using DCF, a probe that fluoresces in response to various types of ROS [44], we recapitulated these findings and demonstrated that the ROS response obtained under these conditions is reduced by CLZ in a concentration-dependent fashion and suppressed at 15 μM (Fig. S2 and Fig. 2A). In addition, CLZ also suppressed the increased $p47^{phox}$ phosphorylation detected at T3, as it can be well appreciated after visualization of the images obtained by confocal microscopy analysis (Fig. 2B). More specifically, phosphorylated $p47^{phox}$-derived fluorescence appeared brighter and organized in patterns extending from the perinuclear region, with a clear labelling of intracellular/nuclear membrane structures (arrows). The diffused labelling detected at T3 + CLZ was like that detected at T0.

An identical outcome was provided by flow cytometric studies (representative cytometric profiles and their quantification are shown in Fig. 2C and D, respectively), which also indicated that this event takes place in the absence of significant changes in the overall $p47^{phox}$ expression (Fig. 2E). Finally, a CLZ-sensitive increased expression of $p67^{phox}$, an additional NOX-2 subunit [54], was also detected at T3 (Fig. 2F).

These results, while further implicating NOX-2 activation in ROS formation occurring at the early stages of SW872 cell differentiation, indicate that this response is suppressed by CLZ as a likely consequence of its ability to cause NOX-2 inhibition.

3.3. Antioxidant activity of clozapine contributes to its suppressive effects on early ROS formation

As previously reported [23–25], CLZ displays an antioxidant activity

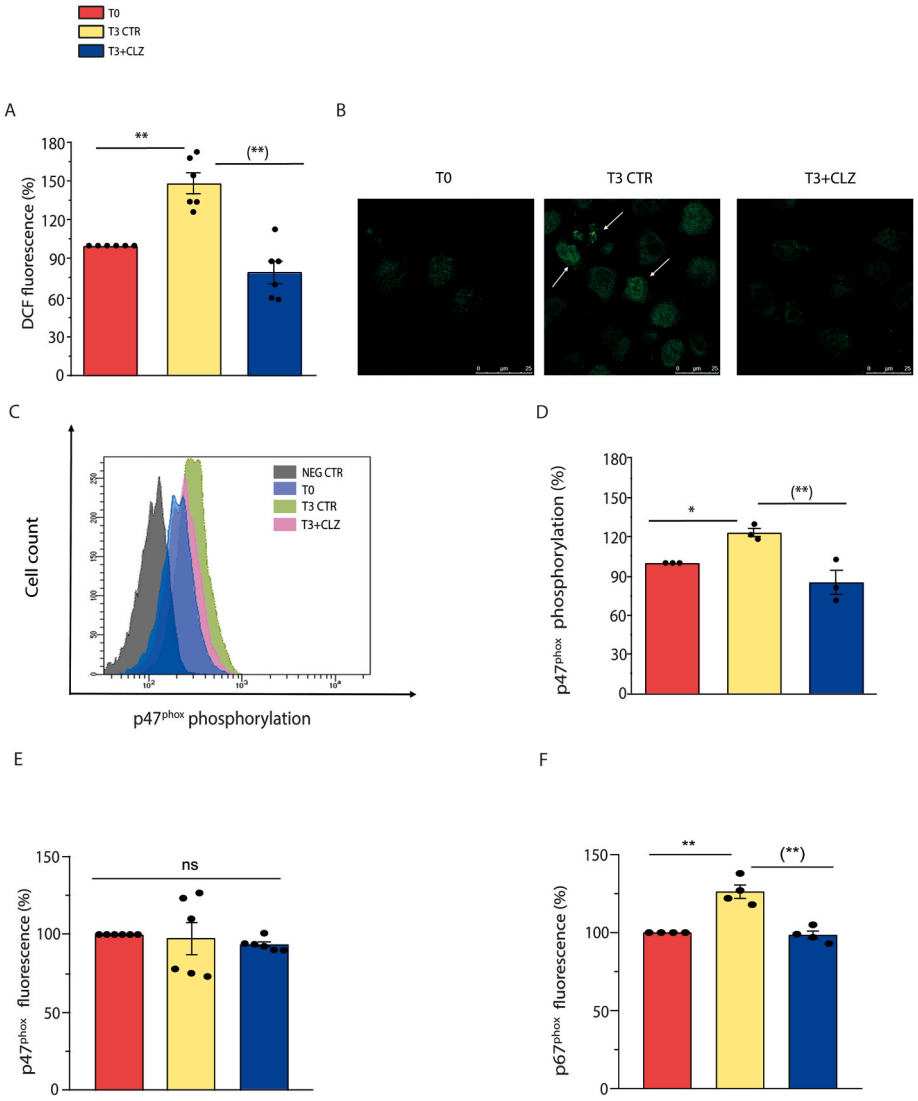

Fig. 2. Clozapine blunts NOX-2-dependent ROS in SW872 cells.
Confluent SW872 cells were induced to differentiate for 3 days with or without CLZ. (A) ROS formation detected with a flow cytometric assay using DCF. (B) Representative micrographs showing phosphorylated $p47^{phox}$ localization (white arrows). In these experiments, the cells were fixed and analysed for immunocytochemical detection of phosphorylated $p47^{phox}$ by confocal microscopy, with all three panels having identical excitation and exposure conditions. Magnification 60X; Scale bar represents 25 μm. (C) Representative flow cytometry histograms of phosphorylated $p47^{phox}$ fluorescence. (D) Statistical analysis of the results obtained in (C). (E–F) Statistical analysis of flow cytometry histograms of $p47^{phox}$ and $p67^{phox}$ fluorescence. T3 CTR received DMSO alone. Data are expressed in % respect to T0 condition. Results represent the means ± SEM calculated from at least three independent determinations. *$p < 0.05$, **$p < 0.01$, as compared to T0; (**)$p < 0.01$, as compared to T3. ns: not significant (one-way ANOVA followed by Dunnett's test).

that might contribute to the observed inhibition of the ROS response. We therefore investigated NOX-2 inhibitory *vs* direct antioxidant effects of CLZ in a well-defined cellular system, i.e., promonocytic U937 cells, that have PMA-responsive NOX-2 activity [55,56]. In these experiments, the cells were initially exposed for 1 or 24 h to CLZ, treated for 15 min with either 0.162 μM PMA or 150 μM H_2O_2, and immediately processed to determine the DCF fluorescence. As indicated in Fig. 3, PMA and H_2O_2 promoted similar fluorescence responses that were suppressed by CLZ supplementation for both 1 (A) and 24 (B) h. These experiments were preceded by preliminary studies, not reported here for the sake of brevity, establishing the H_2O_2 concentration causing a DCF fluorescence response comparable with that elicited by PMA. We also determined that treatments with PMA or H_2O_2 fail to promote loss of membrane integrity and/or apoptotic DNA chromatin fragmentation/condensation (not shown).

We could not perform similar experiments in differentiating SW872 cells, as concomitant ROS formation and activation of various signalling and antioxidant pathways complicates the interpretation of the experimental results. We therefore used undifferentiated SW872 cells and obtained results in line with those from U937 cells. More specifically, the 1 (Fig. 3C) or 24 (Fig. 3D) h exposure protocol to CLZ suppressed the ROS response induced by both 0.162 μM PMA and 750 μM H_2O_2. Note that SW872 cells were particularly resistant to H_2O_2, and that a concentration of the oxidant five times greater than that used in U937 cells was needed to promote a fluorescence response like that mediated by PMA. These differences are not surprising, as remarkable variations in the susceptibility of different cell types have been previously reported by various laboratories and attributed to an array of variables, such as cell density, expression of antioxidant enzymes, growth conditions, etc. [57,58].

We finally performed a luminol-chemiluminescent assay to determine whether, at T3, NOX-2-derived ROS are released in the extracellular milieu and obtained negative results (Fig. S3B) under the same conditions in which as low as 2.5 μM H_2O_2 caused a clear catalase-sensitive signal (Fig. S3A). This is consistent with the notion, also supported by confocal microscopy images shown in Fig. 2B, that NOX-2 is largely compartmentalised in intracellular/nuclear membranes to mediate ROS-dependent signalling regulation.

The last set of experiments illustrated in this section addressed the issue of whether CLZ was capable of mediating antioxidant effects in the extracellular compartment, which turned out to be the case since the chemiluminescence signal emitted by increasing concentrations of H_2O_2 was dramatically reduced by 15 μM CLZ (Fig. S3C).

The results presented in this section are consistent with the possibility that the inhibitory effects mediated by CLZ on SW872 cell differentiation are paralleled by two different activities of the drug converging in suppression of the early ROS signalling, i.e., NOX-2 inhibition and ROS scavenging.

3.4. *Clozapine prevents Nrf2 expression/activation and the ensuing antioxidant response*

We analysed the consequences of the inhibitory effects of CLZ on early ROS formation and initially examined Nrf2 expression. Enhanced mRNA (Fig. 4A) and protein (Fig. 4B) Nrf2 expression was clearly detected in differentiating SW872 cells at T3, in parallel with the translocation of the transcription factor to the nuclei (Fig. 4C). Consistently with the notion that Nrf2 activation leads to enhanced expression of numerous antioxidant genes [59,60], we observed an increased expression of NQO1 (Fig. 4D). The increased levels of cellular GSH (Fig. 4E) are also linked to Nrf2, which controls the expression of glutamate-cysteine ligase (GCL), the rate limiting enzyme of GSH synthesis [61]. Likewise, T3 cells displayed increased expression of Trx-1 (Fig. 4F) and of the corresponding reductase (Fig. 4H), as well as an

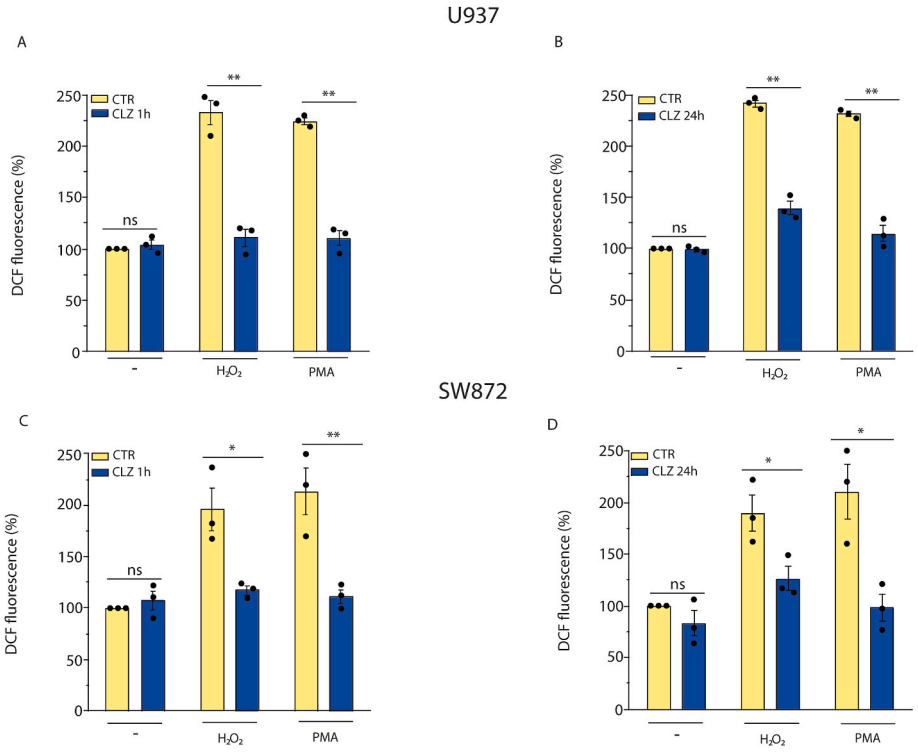

Fig. 3. Antioxidant *vs* NOX-2 inhibitory effects of clozapine in U937 and SW872 cells. U937 cells were treated for 1 h (A) or 24 h (B) with or without CLZ and then exposed for 15 min to either 150 μM H_2O_2 or 0.162 μM PMA. Undifferentiated SW872 cells (C and D) were also used in identical experiments, in which however the concentration of H_2O_2 employed was significantly greater, i.e., 750 μM (30 min) and the exposure time to PMA was 30 min. After treatments, the cells were analysed for DCF fluorescence. CTR samples received DMSO alone. Data are expressed in % respect to untreated CTR cells. Results represent the means ± SEM calculated from at least three independent determinations. *$p < 0.05$, **$p < 0.01$, as compared to CTR cells. ns: not significant (Unpaired *t*-test).

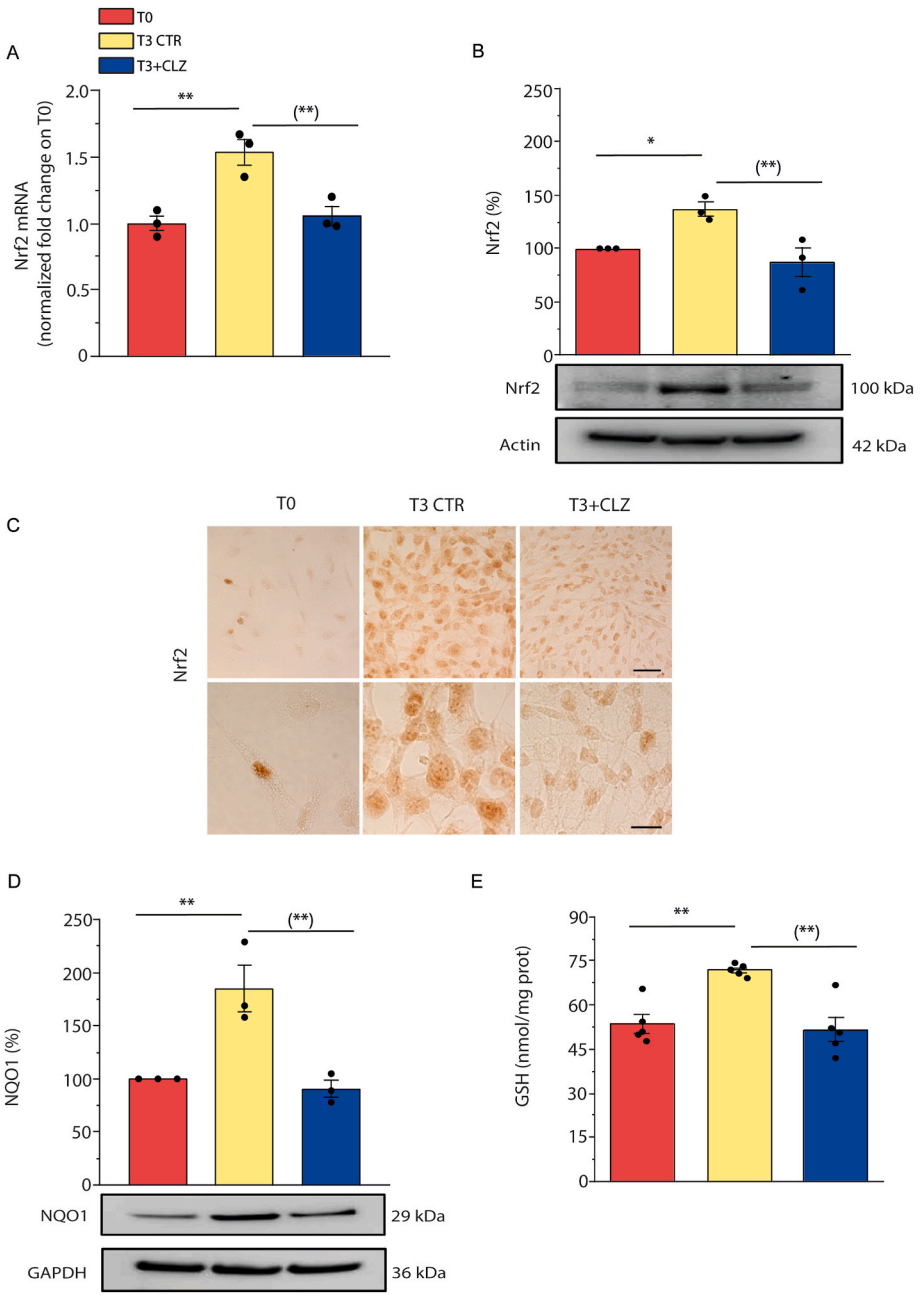

Fig. 4. Clozapine prevents Nrf2 expression and the ensuing antioxidant response in SW872 cells.
Confluent SW872 cells were induced to differentiate for 3 days with or without CLZ (15 μM). (A) Quantitative real time PCR of Nrf2 expression. The graph shows the normalized fold change compared to T0. GAPDH was used as housekeeping. (B) Western immunoblotting analysis of Nrf2 expression. Actin was used as loading control. (C) Immunocytochemical analysis of Nrf2 expression. Magnification 40X and 100X. Scale bars represent 40 and 20 μm. (D) Western immunoblotting analysis of NQO1 expression. GAPDH was used as loading control. (E) GSH content. (F) Western immunoblotting analysis of Trx-1 expression. Actin was used as loading control. (G) Trx-1 activity (expressed as the activity nmol active Trx-1 per mg total protein as inferred from a standard curve with recombinant human Trx-1). (H) Western immunoblotting analysis of TrxR-1 expression. GAPDH was used as loading control. (I) TrxR-1 activity (expressed as the activity pmol active TrxR-1 per mg total protein as inferred from a standard curve with recombinant human TrxR-1). T3 CTR received DMSO alone. Data in the panels B, D, F, and H are expressed in % respect to T0 condition. Results represent the means ± SEM calculated from at least three independent determinations. *$p < 0.05$, **$p < 0.01$, as compared to T0; (*) $p < 0.05$, (**)$p < 0.01$, as compared to T3 (one-way ANOVA followed by Dunnett's test).

increase in the activities of both Trx-1 (Fig. 4G) and TrxR-1 (Fig. 4I).

CLZ blunted Nrf2 expression and the above downstream responses (Fig. 4A–I). CLZ instead failed to directly affect the activity of the Trx system. This notion was established by testing the effect of increasing concentrations of the SGA on the activity of recombinant human TrxR-1 (Fig. S4A), which instead displayed collateral sensitivity to auranofin (Fig. S4B). A high concentration of CLZ (100 μM) also failed to affect recombinant human Trx-1 activity (Fig. S4C).

Asking whether CLZ could redox cycle with the Trx system, similarly to that seen with the peroxidase mimic ebselen [62], we tested whether CLZ could promote the NADPH consumption of the Trx-1/TrxR-1 system *in vitro* in the presence of H_2O_2, which however was not the case (Figs. S5A and B).

Collectively, the results presented in this section indicate that CLZ,

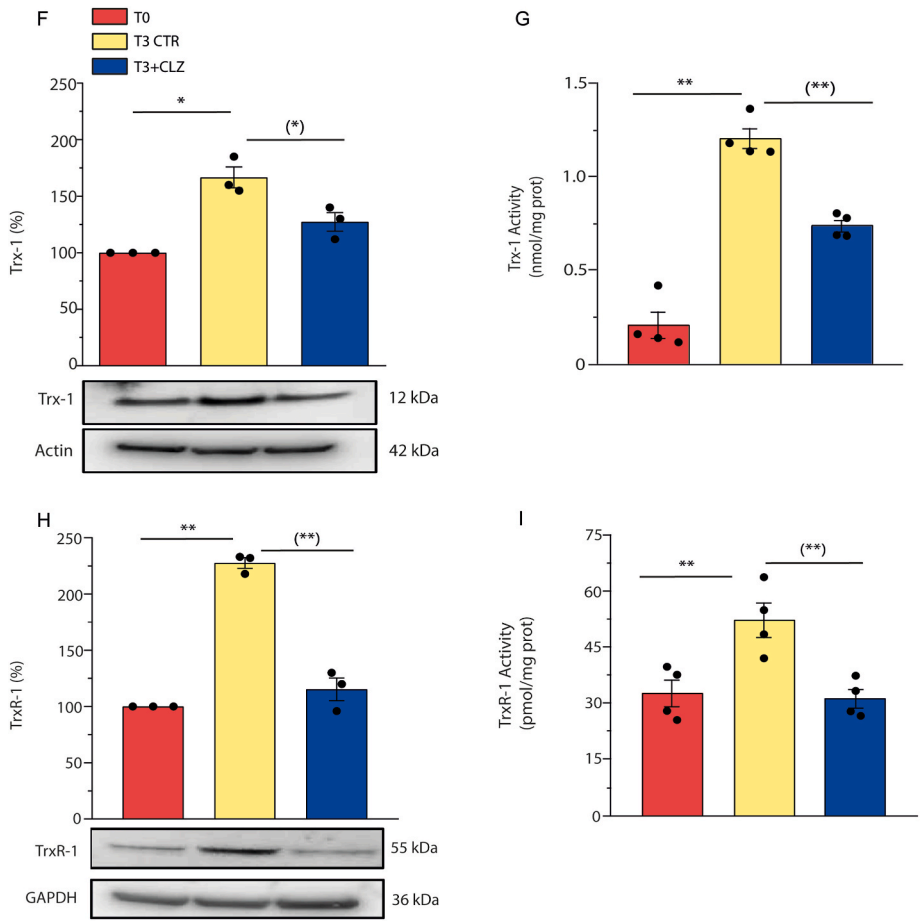

Fig. 4. (*continued*).

by virtue of its ability to inhibit the formation of NOX-2-derived ROS and to scavenge ROS, effectively blunts the Nrf2 signalling.

3.5. Clozapine promotes mitochondrial ROS formation and dysfunction

Adipogenic differentiation of SW872 cells is associated with a late formation of mitochondrial ROS, particularly significant at T10 [33]. CLZ, by blunting the early Nrf2 antioxidant signalling, could anticipate the formation of these ROS and thus distort the intracellular signalling events. On the other hand, the potent antioxidant effects of CLZ, if also displayed in the intramitochondrial compartment, might blunt mitochondrial ROS. These alternatives were next addressed.

To obtain an indication on the impact of the antioxidant activity of CLZ on mitochondrial ROS, we employed once again U937 cells grown for 1 or 24 h with or without CLZ, followed by a final 10 min treatment with 2.5 μM arsenite/100 μM ATP. This cocktail promotes the exclusive formation of mitochondrial superoxide [41] and, not surprisingly, elicited a significant MitoSOX-red fluorescence signal (Fig. 5A and B). This MitoSOX-red fluorescence response was not affected by the 1 h CLZ supplementation protocol (Fig. 5A). Furthermore, there was a significantly increased fluorescent signal in cells that had also received CLZ for 24 h (Fig. 5B).

This indicates that CLZ fails to scavenge mitochondrial ROS, or can even increase their levels, in contrast to the opposite effects in the cytosol shown above (Fig. 3). We thus also performed experiments using DCF, which detects ROS in the cytosol, upon the same 2.5 μM arsenite/100 μM ATP supplementation. Under these conditions, the DCF fluorescent signal should be due to cytosolic H_2O_2 derived from mitochondrial superoxide [41]. In contrast to the results obtained with MitoSOX-Red, CLZ completely suppressed the DCF fluorescence in this case, in cells supplemented with the drug for 1 (Fig. 5C) or 24 (Fig. 5D) h, respectively.

Thus, CLZ is an effective scavenger of ROS in the cytosolic compartment, regardless of their origin, but not in the mitochondrial compartment. With this information in mind, we next moved to experiments investigating the impact of CLZ on mitochondrial ROS formation in differentiating SW872 cells. As expected, there was no difference in the percentage of MitoSOX-red positive cells at T0 *vs* T3 (Fig. 6A) as well as in the overall fluorescence response (Fig. 6B). Interestingly, however, CLZ significantly increased both effects.

Our findings are therefore consistent with the possibility that suppression of early NOX-2-derived ROS, and of the ensuing stimulation of the Nrf2 antioxidant response, lowers the efficiency of the mitochondrial antioxidant machinery, thereby fostering mitochondrial ROS formation.

To address the issue of the consequences of the early mitochondrial ROS formation, we focused on Trx-2, which, while Nrf2-independent, was increased at T3 in control cells *via* a mechanism sensitive to CLZ (Fig. 6C). Interestingly, under the same conditions CLZ also increased Trx-2 oxidation, as indicated by the outcome of Trx-2 redox state gel assays, using diamide as a positive control (Fig. 6D). However, CLZ did not affect human Trx-2 activity *in vitro* using pure enzyme systems (Fig. S4D).

Fig. 6E shows that CLZ blunts the increased NAO fluorescence detected at T3, indicative of an increased cardiolipin expression. This effect of CLZ is compatible with inhibition of mitochondrial biogenesis and with cardiolipin oxidation. Furthermore, confocal microscopy studies indicated that CLZ promotes mitochondrial fragmentation and a general disorganization of the mitochondrial network, which was not as evidently observed in the absence of CLZ (Fig. 6F and S6).

Together, these results indicate that CLZ promotes an anticipated

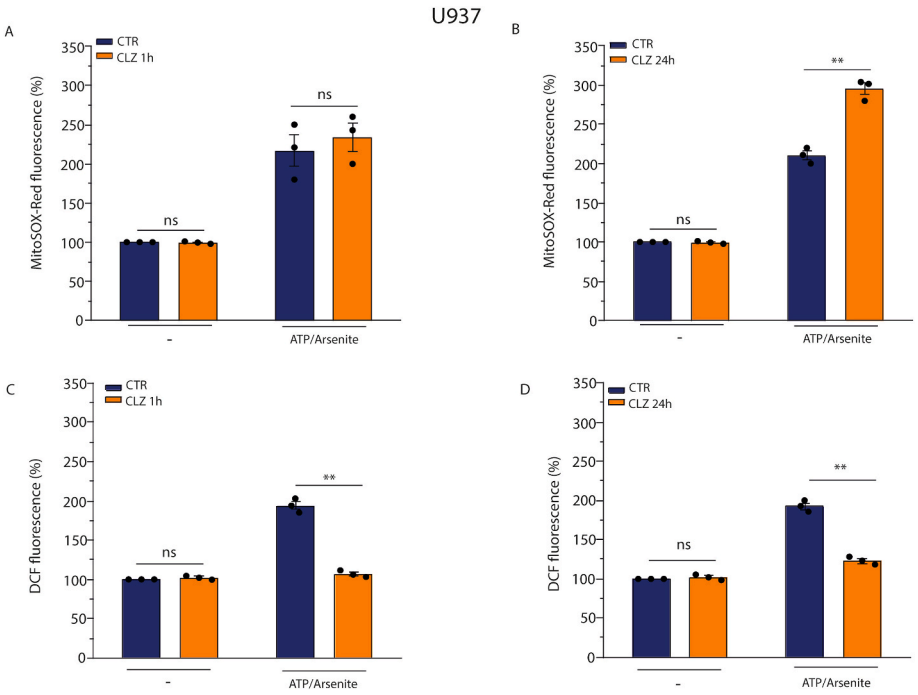

Fig. 5. Clozapine fails to promote an antioxidant effect in the intramitochondrial compartment in U937 cells.
U937 cells were treated for 1 h (A and C) or 24 h (B and D) with or without CLZ and then exposed for 10 min to 100 μM ATP/2.5 μM arsenite. Cells were finally analysed for ROS formation with either MitoSOX-red (A and B) or DCF (C and D). CTR samples received DMSO alone. Data are expressed as % of untreated CTR cells. Results represent the means ± SEM calculated from at least three independent determinations. **p < 0.01 as compared to CTR cells; ns: not significant (Unpaired *t*-test). (For interpretation of the references to colour in this figure legend, the reader is referred to the Web version of this article.)

mitochondrial ROS formation and hence causes mitochondrial dysfunction during the early stages of SW872 cell adipogenic differentiation.

3.6. The effects of clozapine on primary mouse embryonic fibroblast adipogenic differentiation

We performed experiments to determine whether some of the key findings obtained with SW872 cells could be recapitulated in primary cells. For this purpose, we used MEFs, previously shown to undergo adipogenic differentiation when grown in an appropriate DM [63–67]. Adipogenic differentiation of these cells was measured at T3, to minimize the variables with the experiments performed in SW872 cells. We initially provided evidence of lipid accumulation using BODIPY (Fig. 7A–B) and NR (Fig. 7C–D), two fluorescent probes allowing visualization and quantification of LDs, by fluorescence microscopy and flow cytometry, respectively. Qualitative indication of adipogenic differentiation was then provided by ORO-staining experiments (Fig. 7E). Also note that the level of ORO-staining increased further at T4 (Fig. S7A).

Adipogenic differentiation of MEFs was also measured at the molecular level, by documenting an increased mRNA expression of relevant transcription factors (C/EBPβ, C/EBPδ, C/EBPα, PPARγ, GLUT4) at T3 (Fig. 7F) and their further increase at T4 (Fig. S7B). Moreover, C/EBPβ (Fig. 7G) and PPARγ (Fig. S7C) protein expression, respectively detected by WB and cytochemical analyses, as well as DCF fluorescence (Fig. 7H), were significantly increased at T3.

All together, the above results demonstrated that MEFs were grown under conditions leading to adipogenic differentiation and early ROS formation.

We therefore investigated the effects of CLZ (15 μM) and found that the SGA slowed down adipogenesis (Fig. 7), as detected with BODIPY (A and B) and NR-cytofluorimetric analysis (C and D), as well as with ORO-staining (E). CLZ also suppressed the increased mRNA expression of the main adipogenic transcription factors (Fig. 7F) and C/EBPβ protein expression (Fig. 7G).

In other assays, we confirmed the ability of CLZ to blunt the DCF fluorescence response (Fig. 7H) and to anticipate mitochondrial ROS formation (Fig. 7I).

The last set of experiments was performed to address the issue of whether CLZ displays NOX-2 inhibitory/ROS scavenging effects also in undifferentiated MEFs. As reported in Fig. S8, the SGA suppressed the DCF fluorescence signal induced by 0.162 μM PMA or 100 μM H_2O_2, using both the 1 (A) and 24 (B) h exposure protocol. Note that all the above experiments were performed under conditions in which flow cytometric analysis failed to reveal sub-diploid peaks (Fig. S9A) and toxicity (Fig. S9B) in cells grown with or without CLZ.

It therefore appears that in the MEF model of adipogenic differentiation, CLZ promotes the same critical effects previously described in human SW872 cells, an observation that validates the conclusion of our investigation, i.e., that CLZ slows down adipogenesis and anticipates mitochondrial ROS formation and dysfunction because of the early prevention of formation/scavenging of cytosolic ROS.

4. Discussion

The notion that ROS are critically involved in the adipogenic process is well established [68–70]. In a previous study [33] using the same cells and conditions employed in the present investigation, we identified two separate mechanisms of ROS formation [33], with the first occurring early in differentiation (T3), attributable to NOX-2 activation, and the second one confined to a late phase (T10), in which mitochondria were actively involved.

The increased Nrf2 expression detected at T3 was coincidental with NOX-2-derived superoxide formation, thereby suggesting the existence of a cause-effect relationship. It is well established that mitochondrial superoxide readily dismutates to diffusible H_2O_2 [71], which can then promote extramitochondrial events leading to Nrf2 activation/increased expression. Indeed, the oxidant causes the dissociation of Keap1 from

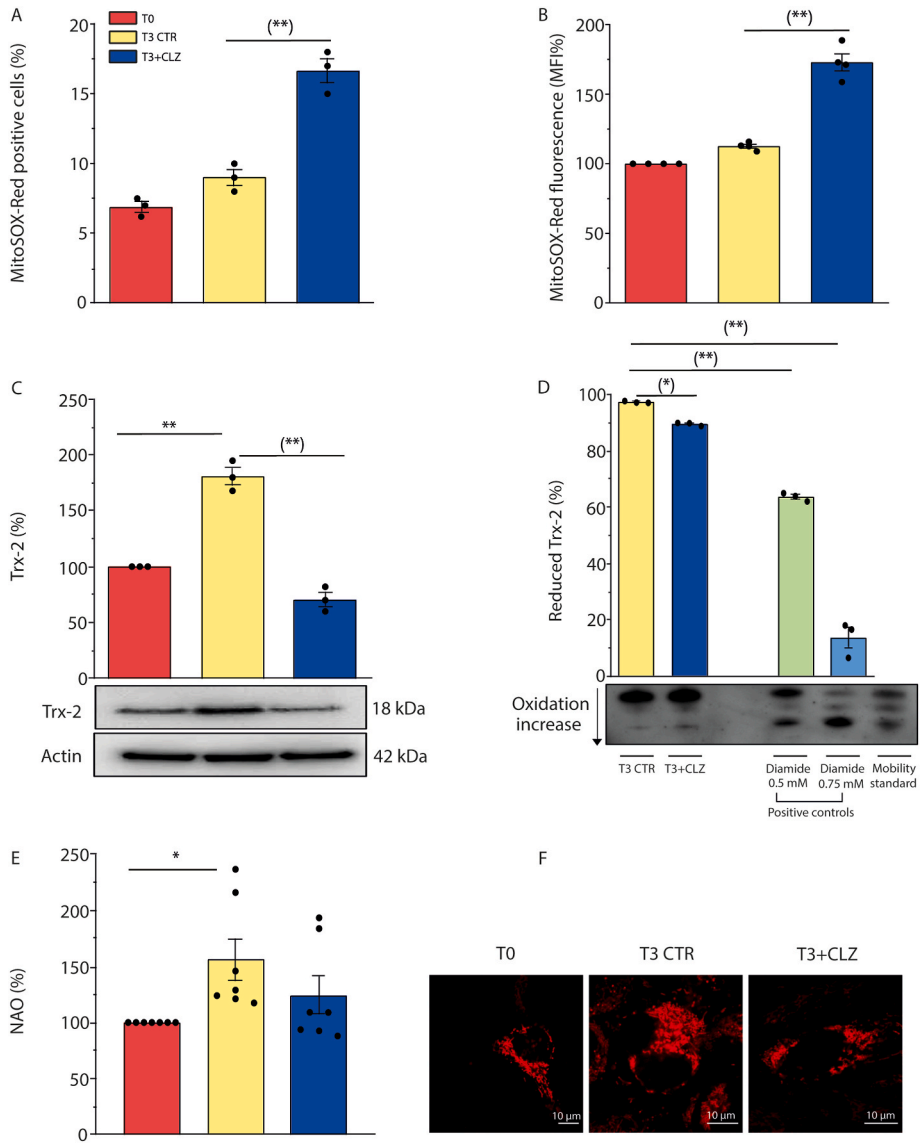

Fig. 6. Clozapine promotes mitochondrial ROS formation and dysfunction in SW872 cells.
Confluent SW872 cells were induced to differentiate for 3 days with or without CLZ. (A) % of MitoSOX-red positive cells (B) Statistical analysis of total MitoSOX-red fluorescence intensity. (C) Western immunoblotting analysis of Trx-2 expression. Actin was used as loading control. (D) Reduced, partially oxidized, and fully oxidized Trx-2 thiol groups. The redox state of Trx-2 was determined by urea polyacrylamide gel electrophoresis under non reducing conditions. Data are expressed as % of T3. (E) NAO analysis. (F) Representative micrographs of mitochondrial network and structural integrity. Images were obtained by confocal microscopy. Magnification 60X; scale bars represent 10 µm. T3 CTR received DMSO alone. Data in the panels B, C and E are expressed in % respect to T0 condition. Results represent the means ± SEM calculated from at least three independent determinations. *$p < 0.05$, **$p < 0.01$, as compared to T0; (*)$p < 0.05$, (**)$p < 0.01$, as compared to T3 (one-way ANOVA followed by Dunnett's test). (For interpretation of the references to colour in this figure legend, the reader is referred to the Web version of this article.)

Nrf2, either by direct oxidation of critical cysteines of Keap1 itself [72], or *via* phosphorylation mediated by a variety of kinases [72,73]. Subsequently, Nrf2 translocates to the nucleus thereby increasing the expression of an array of genes encoding proteins with diverse functions and activities, as antioxidant enzymes regulating the redox state in both the cytosolic and mitochondrial compartments [60].

Consistently with the above premise, we herein report evidence for an early increase in the expression and activity of Trx-1 and TrxR-1, expression of NQO1 and GSH levels, as a likely consequence of the increased expression of GCL, the rate limiting enzyme of GSH biosynthesis [61]. The observation that CLZ suppresses both NOX-2-derived ROS and Nrf2 expression, as well as the expression of Nrf2 dependent antioxidant enzymes, therefore suggests that these events are sequentially connected and causally linked. Consistently, we did not observe direct inhibitory effects of CLZ on the activities of antioxidant enzymes as TrxR-1 or Trx-1.

We also obtained evidence for a similar relationship between NOX-2-derived ROS and progression of adipogenesis, since lipid accumulation was lower in T3 cells supplemented with CLZ, an effect paralleled by inhibition of the expression or nuclear translocation of C/EBPβ or PPARγ, respectively. Although more studies are necessary to univocally implicate Nrf2 in these processes, it is tempting to speculate that the effects of NOX-2-derived ROS on C/EBPβ and PPARγ are mediated by Nrf2, as recently proposed by others [74], which could explain the inhibitory effects of CLZ.

These results provide relevant information on the mechanism(s) involved in the regulation of adipogenic differentiation of SW872 cells. More specifically, it appears that ROS generated by NOX-2 critically

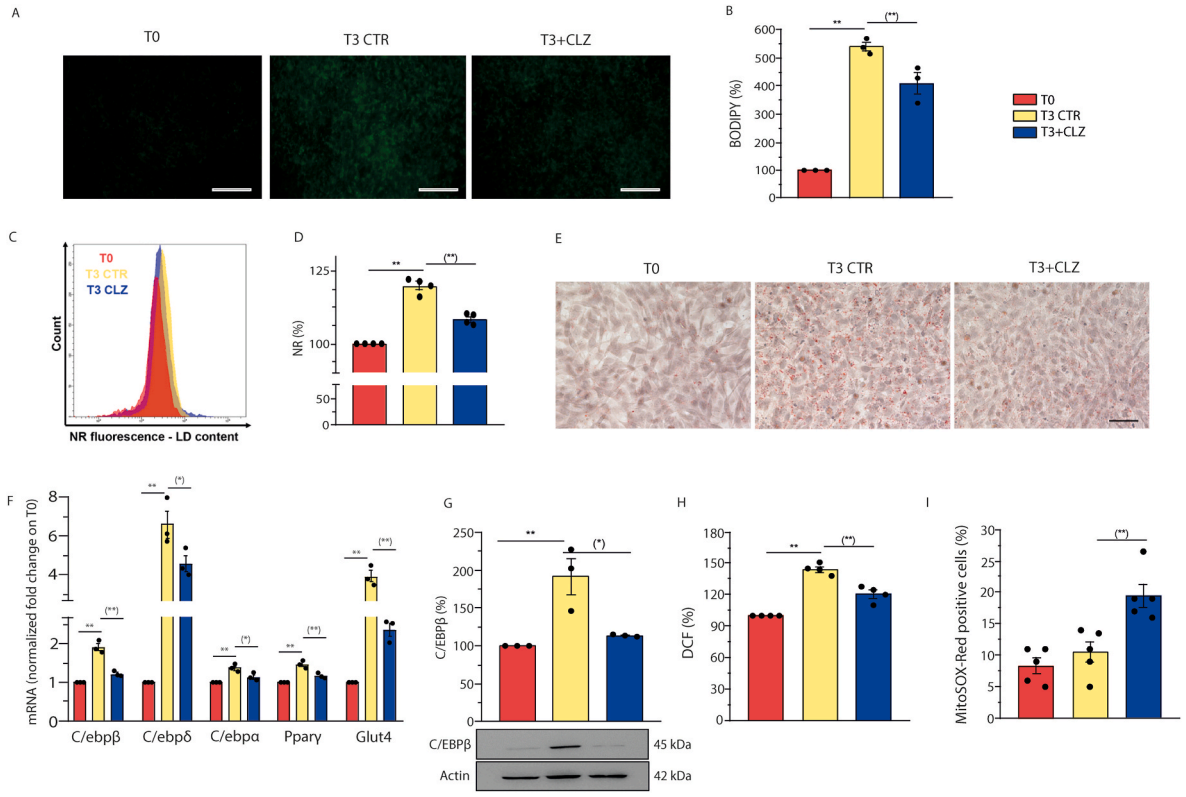

Fig. 7. Clozapine slows down adipogenesis and anticipates mitochondrial ROS formation and dysfunction in MEFs.
Confluent MEFs were induced to differentiate for 3 days with or without CLZ (15 μM). (A) Representative images (40X) of BODIPY-stained LDs in differentiating MEFs. Scale bar = 100 μm. (B) BODIPY fluorescence quantification of (A). (C) Representative flow cytometry histograms of NR-labelled cells in differentiating MEFs. (D) Statistical analysis of the results obtained from NR flow cytometry assays. (E) Representative images (40X) of ORO-stained LDs (red) and hematoxylin-stained nuclei (blue). Scale bar = 50 μm. (F) Quantitative real time PCR of CEBP/β, CEBP/δ, CEBP/α, PPARγ and GLUT4 mRNA expression. The graph shows the normalized fold change compared to T0. HPRT was used as housekeeping. (G) Western immunoblotting analysis of C/EBPβ. Actin was used as loading control. (H) ROS formation detected with a flow cytometric assay using DCF. (I) % of MitoSOX red positive cells. T3 CTR received DMSO alone. Data in panels B, D, G and H are expressed in % respect to T0 condition. Results represent the means ± SEM calculated from at least three independent determinations, **$p < 0.01$, as compared to T0; (*) $p < 0.05$, (**) $p < 0.01$, as compared to T3 (one-way ANOVA followed by Dunnett's test). (For interpretation of the references to colour in this figure legend, the reader is referred to the Web version of this article.)

mediate the triggering of early events regulating an amplification of the overall antioxidant defense and adipocyte differentiation.

We also addressed the mechanism(s) involved in the above effects of CLZ and obtained results suggesting the existence of a dual mechanism based on both NOX-2 inhibition and ROS scavenging.

The notion that CLZ inhibits NOX-2 activity has been previously documented [22,75]. We herein report that, at T3, the SGA suppresses the increased phosphorylation of $p47^{phox}$, mainly detected in intracellular membrane compartments, at variance with phagocytic cells, in which NOX-2 subunits mainly translocate to the plasma membrane compartment during activation [76].

CLZ inhibited $p47^{phox}$ phosphorylation in the absence of detectable changes in $p47^{phox}$ expression. $p47^{phox}$ phosphorylation on specific serine residues was previously documented, and this event has been recently associated with the effects of $p67^{phox}$ [54], which is transcriptionally regulated [77]. Consistently, a dramatic reduction in $p47^{phox}$ phosphorylation was observed in lymphocytes from p67 $^{phox-/-}$ Chronic Granulomatous disease patients [54].

We found that, at T3, cells display an increased expression of $p67^{phox}$ and that this response is suppressed by CLZ, an observation providing a potential link between the decline in $p47^{phox}$ phosphorylation and the diminished $p67^{phox}$ expression.

We also tried to gather information on the antioxidant effects of CLZ and for this purpose employed promonocytic U937 cells, previously shown to respond to PMA with NOX-2-mediated ROS formation [55,56] and SW872 pre-adipocytes, obtaining similar ROS responses. The outcome of these and other studies, in which PMA was replaced with reagent H_2O_2, provided clear evidence for an important and long-lasting antioxidant effect of CLZ, which, in concert with NOX-2 inhibition, may account for the observed effects of CLZ on early ROS signalling. In addition, we showed that CLZ is an effective potential scavenger of extracellular ROS, an effect of a yet undefined significance due to the apparent lack of extracellular ROS at T3, which appears to be consistent with the observed expression of the NOX-2 enzyme in intracellular membrane compartments of adipocytes.

We then addressed the issue of whether the powerful antioxidant effects of CLZ might conceal the expected consequences of prevention of the Nrf2-dependent amplification of antioxidant enzymes, with special reference to the mitochondrial compartment. Mitochondrial ROS formation should indeed take place under growth conditions causing an oversupply of electrons to the respiratory chain [78,79] and prevention of Nrf2 expression should anticipate the formation of these species and make cells more vulnerable to mitochondrial dysfunction. Indeed, Nrf2 is not only a master regulator of cellular redox homeostasis, since, as well summarised in Ref. [80], it also regulates critical mitochondrial functions, which include the efficiency for ATP synthesis, as well as mitochondrial biogenesis and integrity. In this perspective, Nrf2, while not directly involved in the regulation of Trx-2 expression, might nevertheless indirectly control its expression, an event readily observed in differentiating SW872 cells at T3.

In principle, the lipophilic nature of CLZ should be permissive for its mitochondrial uptake, thereby potentially allowing effective scavenging

of mitochondrial ROS, but apparently this might not the case, since CLZ failed to reduce the MitoSOX-red fluorescence response selectively induced by the cocktail ATP/arsenite in U937 or SW872 cells. This was an interesting observation, since under the same conditions CLZ instead scavenged mitochondrial ROS-derived H_2O_2 in the cytosolic compartment, in keeping with previous findings obtained in experiments using reagent H_2O_2.

Based on the above considerations, we were not surprised to observe that CLZ remarkably anticipates mitochondrial ROS formation at T3, with no evidence of cytosolic ROS, either mediated by NOX-2 or derived from mitochondrial ROS.

The obvious consequence of early mitochondrial ROS formation in cells made vulnerable by the impaired Nrf2 response was the induction of signs of mitochondrial dysfunction. We indeed demonstrated that these events were associated with a reorganization of the mitochondrial network with clear morphological evidence of fragmentation. At the biochemical level, these events were associated with Trx-2 oxidation, a well-established and critical intramitochondrial target [42]. At least in principle, the results obtained in experiments measuring cardiolipin expression are also suggestive of cardiolipin oxidation induced by mitochondrial ROS, an additional important mitochondrial target.

These findings are however of more complex interpretation as increased cardiolipin expression detected at T3 likely reflects increased mitochondrial biogenesis which accompanies adipogenesis [81]. The inhibitory effects of CLZ might therefore suggest that the SGA blunts mitochondrial biogenesis, which also represents a good explanation for our results on Trx-2 expression, increased at T3 *via* a CLZ-sensitive mechanism. Our results on Nrf2 expression are also consistent with the possibility that CLZ inhibits mitochondrial biogenesis, as Nrf2 is a positive regulator of this process [81]. Finally, confocal images shown in Fig. S6 are compatible with an increased mitochondrial biogenesis detected at T3, significantly reduced by CLZ.

Thus, we herein provide results showing that the anticipated mitochondrial ROS formation triggered by CLZ at T3 promotes some early signs of mitochondrial dysfunction. On the other hand, our results also suggest that CLZ inhibits mitochondrial biogenesis, an effect currently investigated in our laboratories. Impairment of mitochondrial biogenesis and mitochondrial disfunction are indeed strictly related processes in pathological adipogenesis, and critically connected with metabolic diseases and obesity [82].

As a final note, we could replicate the same critical effects described above in a different model of adipogenic differentiation, with different characteristics, i.e., MEFs, of murine origin unlike SW872 cells, which are human. Furthermore, MEFs are primary cells in contrast to SW872 cells, a continuous cell line derived from a liposarcoma.

Thus, the results presented in this study indicate that CLZ blunts early NOX-2 derived ROS, thereby preventing Nrf2 expression and activation, and slowing down adipogenesis. These conditions are then associated with a significantly anticipated formation of mitochondrial ROS, with the SGA displaying antioxidant properties restricted to the cytosolic compartment. CLZ therefore causes an early mitochondrial dysfunction in differentiating adipocytes, an event critically connected with metabolic syndrome associated pathologies.

Fig. 8 summarises this proposed scheme, which may help to explain how CLZ has its unique and sometimes grave adverse metabolic effects when used in the clinical setting.

Author contributions

MF, EA, and OC conceived and designed the study.

MF, G Blandino, G Buffi, BC, RDM, LC, AG, and MM conducted experimental work and data acquisition.

MF, G Blandino, G Buffi, RDM, BC, LC, AG, EA, and OC analysed and interpreted the results.

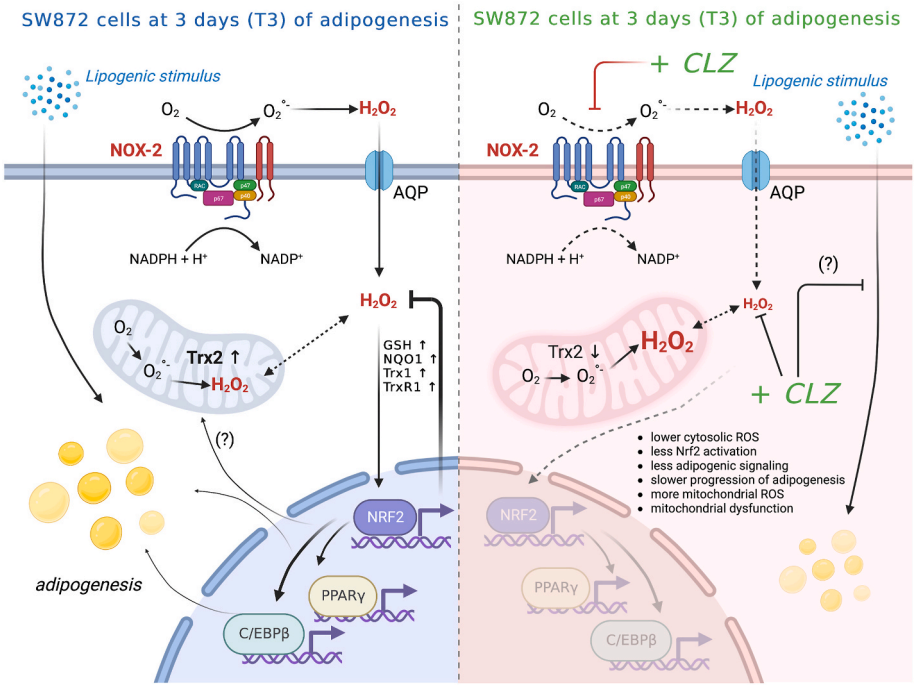

Fig. 8. Schematic summary of the proposed mechanism of clozapine on induction of early mitochondrial dysfunction.
Early adipogenic differentiation of human SW872 cells is accompanied by activation of NOX-2 and superoxide formation. In this scheme the components of NOX-2 enzyme are associated with the plasma membrane, although localization in other membranes (e.g., nuclear membrane) is also possible [83]. Dismutation of superoxide to H_2O_2 triggers Nrf2 activation and a plethora of downstream events associated with the amplification of the antioxidant machinery, maintenance of mitochondrial function and integrity and, possibly, stimulation of the adipogenic signalling. CLZ suppressed ROS formation by a dual mechanism, based on both NOX-2 inhibition and ROS scavenging restricted to the cytosolic compartment, thereby preventing Nrf2 activation and the above downstream events. These conditions were associated with mitochondrial ROS formation, resistant to the antioxidant effects of CLZ, and by signs of an early mitochondrial dysfunction. This figure was edited according to the licence agreement: "Created with BioRender.com".

MF and OC wrote the manuscript.

MF, EA, G Blandino, G Buffi, LC, and OC reviewed, wrote, and edited the final manuscript.

All authors discussed the results and contributed to the final manuscript.

Funding

This work was supported by Ricerca Finalizzata—Ministero della salute 2018 (RF-2016-02363761)—Italy and by Karolinska Institutet, The Knut and Alice Wallenberg Foundations (KAW 2019.0059), The Swedish Cancer Society (21 1463 Pj), The Swedish Research Council (2021–02214), The Cayman Biomedical Research Institute (CABRI), The Hungarian Thematic Excellence Programme (TKP2021-EGA-44), The Hungarian National Research, Development and Innovation Office (ED_18-1-2019-0025), and The Hungarian National Tumor Biology Laboratory.

Conflict of Interest disclosure: The authors declare no potential conflict of interest.

Declaration of competing interest

The authors declare that they have no known competing financial interests or personal relationships that could have appeared to influence the work reported in this paper.

Data availability

Data will be made available on request.

Appendix A. Supplementary data

Supplementary data to this article can be found online at https://doi.org/10.1016/j.redox.2023.102915.

References

[1] A.T. Raben, V.S. Marshe, A. Chintoh, I. Gorbovskaya, D.J. Muller, M.K. Hahn, The complex relationship between antipsychotic-induced weight gain and therapeutic benefits: a systematic review and implications for treatment, Front. Neurosci. 11 (2017) 741.

[2] E. Fernandez-Egea, C. Garcia-Rizo, B. Miller, E. Parellada, A. Justicia, M. Bernardo, B. Kirkpatrick, Testosterone in newly diagnosed, antipsychotic-naive men with nonaffective psychosis: a test of the accelerated aging hypothesis, Psychosom. Med. 73 (8) (2011) 643–647.

[3] P. Oriot, J.L. Feys, S. Mertens de Wilmars, A. Misson, L. Ayache, O. Fagnart, D. Gruson, A. Luts, J. Jamart, M.P. Hermans, M. Buysschaert, Insulin sensitivity, adjusted beta-cell function and adiponectinaemia among lean drug-naive schizophrenic patients treated with atypical antipsychotic drugs: a nine-month prospective study, Diabetes Metabol. 34 (5) (2008) 490–496.

[4] C.C. Chiu, K.P. Chen, H.C. Liu, M.L. Lu, The early effect of olanzapine and risperidone on insulin secretion in atypical-naive schizophrenic patients, J. Clin. Psychopharmacol. 26 (5) (2006) 504–507.

[5] J.W.Y. Yuen, D.D. Kim, R.M. Procyshyn, W.J. Panenka, W.G. Honer, A.M. Barr, A focused review of the metabolic side-effects of clozapine, Front. Endocrinol. 12 (2021), 609240.

[6] J.A. Lieberman, T.S. Stroup, J.P. McEvoy, M.S. Swartz, R.A. Rosenheck, D. O. Perkins, R.S. Keefe, S.M. Davis, C.E. Davis, B.D. Lebowitz, J. Severe, J.K. Hsiao, I. Clinical, Antipsychotic Trials of Intervention Effectiveness, Effectiveness of antipsychotic drugs in patients with chronic schizophrenia, N. Engl. J. Med. 353 (12) (2005) 1209–1223.

[7] H. Nasrallah, A review of the effect of atypical antipsychotics on weight, Psychoneuroendocrinology 28 (Suppl 1) (2003) 83–96.

[8] S. Leucht, C. Corves, D. Arbter, R.R. Engel, C. Li, J.M. Davis, Second-generation versus first-generation antipsychotic drugs for schizophrenia: a meta-analysis, Lancet 373 (9657) (2009) 31–41.

[9] A.H. Barnett, P. Mackin, I. Chaudhry, A. Farooqi, R. Gadsby, A. Heald, J. Hill, H. Millar, R. Peveler, A. Rees, V. Singh, D. Taylor, J. Vora, P.B. Jones, Minimising metabolic and cardiovascular risk in schizophrenia: diabetes, obesity and dyslipidaemia, J. Psychopharmacol. 21 (4) (2007) 357–373.

[10] J.L. Roerig, K.J. Steffen, J.E. Mitchell, Atypical antipsychotic-induced weight gain: insights into mechanisms of action, CNS Drugs 25 (12) (2011) 1035–1059.

[11] G. Tulipano, C. Rizzetti, I. Bianchi, A. Fanzani, P. Spano, D. Cocchi, Clozapine-induced alteration of glucose homeostasis in the rat: the contribution of hypothalamic-pituitary-adrenal axis activation, Neuroendocrinology 85 (2) (2007) 61–70.

[12] Y.E. Savoy, M.A. Ashton, M.W. Miller, F.M. Nedza, D.K. Spracklin, M.H. Hawthorn, H. Rollema, F.F. Matos, E. Hajos-Korcsok, Differential effects of various typical and atypical antipsychotics on plasma glucose and insulin levels in the mouse: evidence for the involvement of sympathetic regulation, Schizophr. Bull. 36 (2) (2010) 410–418.

[13] L. Benarroch, C. Kowalchuk, V. Wilson, C. Teo, M. Guenette, A. Chintoh, Y. Nesarajah, V. Taylor, P. Selby, P. Fletcher, G.J. Remington, M.K. Hahn, Atypical antipsychotics and effects on feeding: from mice to men, Psychopharmacology 233 (14) (2016) 2629–2653.

[14] C. Cuerda, J. Merchan-Naranjo, C. Velasco, A. Gutierrez, M. Leiva, M.J. de Castro, M. Parellada, M. Giraldez, I. Breton, M. Camblor, P. Garcia-Peris, E. Dulin, I. Sanz, M. Desco, C. Arango, Influence of resting energy expenditure on weight gain in adolescents taking second-generation antipsychotics, Clin. Nutr. 30 (5) (2011) 616–623.

[15] M.R. Baig, E. Navaira, M.A. Escamilla, H. Raventos, C. Walss-Bass, Clozapine treatment causes oxidation of proteins involved in energy metabolism in lymphoblastoid cells: a possible mechanism for antipsychotic-induced metabolic alterations, J. Psychiatr. Pract. 16 (5) (2010) 325–333.

[16] C. Walss-Bass, S.T. Weintraub, J. Hatch, J. Mintz, A.R. Chaudhuri, Clozapine causes oxidation of proteins involved in energy metabolism: a possible mechanism for antipsychotic-induced metabolic alterations, Int. J. Neuropsychopharmacol. 11 (8) (2008) 1097–1104.

[17] E.L. Streck, G.T. Rezin, L.M. Barbosa, L.C. Assis, E. Grandi, J. Quevedo, Effect of antipsychotics on succinate dehydrogenase and cytochrome oxidase activities in rat brain, N. Schmied. Arch. Pharmacol. 376 (1–2) (2007) 127–133.

[18] V. Contreras-Shannon, D.L. Heart, R.M. Paredes, E. Navaira, G. Catano, S.K. Maffi, C. Walss-Bass, Clozapine-induced mitochondria alterations and inflammation in brain and insulin-responsive cells, PLoS One 8 (3) (2013), e59012.

[19] P. Sangwung, K.F. Petersen, G.I. Shulman, J.W. Knowles, Mitochondrial dysfunction, insulin resistance, and potential genetic implications, Endocrinology 161 (4) (2020).

[20] J.A. Kim, Y. Wei, J.R. Sowers, Role of mitochondrial dysfunction in insulin resistance, Circ. Res. 102 (4) (2008) 401–414.

[21] H.Q. Tran, S.J. Park, E.J. Shin, T.V. Tran, N. Sharma, Y.J. Lee, J.H. Jeong, C. G. Jang, D.J. Kim, T. Nabeshima, H.C. Kim, Clozapine attenuates mitochondrial burdens and abnormal behaviors elicited by phencyclidine in mice via inhibition of p47 (phox); Possible involvements of phosphoinositide 3-kinase/Akt signaling, J. Psychopharmacol. 32 (11) (2018) 1233–1251.

[22] L. Jiang, X. Wu, S. Wang, S.H. Chen, H. Zhou, B. Wilson, C.Y. Jin, R.B. Lu, K. Xie, Q. Wang, J.S. Hong, Clozapine metabolites protect dopaminergic neurons through inhibition of microglial NADPH oxidase, J. Neuroinflammation 13 (1) (2016) 110.

[23] A. Dalla Libera, G. Scutari, R. Boscolo, M.P. Rigobello, A. Bindoli, Antioxidant properties of clozapine and related neuroleptics, Free Radic. Res. 29 (2) (1998) 151–157.

[24] I. Sadowska-Bartosz, S. Galiniak, G. Bartosz, M. Zuberek, A. Grzelak, A. Dietrich-Muszalska, Antioxidant properties of atypical antipsychotic drugs used in the treatment of schizophrenia, Schizophr. Res. 176 (2–3) (2016) 245–251.

[25] F.F. Brinholi, C.C. Farias, K.L. Bonifacio, L. Higachi, R. Casagrande, E.G. Moreira, D.S. Barbosa, Clozapine and olanzapine are better antioxidants than haloperidol, quetiapine, risperidone and ziprasidone in in vitro models, Biomed. Pharmacother Biomedecine & pharmacotherapie 81 (2016) 411–415.

[26] B.R. Imhoff, J.M. Hansen, Differential redox potential profiles during adipogenesis and osteogenesis, Cell. Mol. Biol. Lett. 16 (1) (2011) 149–161.

[27] X. Wang, C. Hai, Redox modulation of adipocyte differentiation: hypothesis of "Redox Chain" and novel insights into intervention of adipogenesis and obesity, Free Radic. Biol. Med. 89 (2015) 99–125.

[28] X. Peng, A. Gimenez-Cassina, P. Petrus, M. Conrad, M. Ryden, E.S. Arner, Thioredoxin reductase 1 suppresses adipocyte differentiation and insulin responsiveness, Sci. Rep. 6 (2016), 28080.

[29] V. Ferreira, D. Grajales, A.M. Valverde, Adipose tissue as a target for second-generation (atypical) antipsychotics: a molecular view, Biochimica et biophysica acta, Mol. Cell Biol. Lipids 1865 (2) (2020), 158534.

[30] T. Tsubai, A. Yoshimi, Y. Hamada, M. Nakao, H. Arima, Y. Oiso, Y. Noda, Effects of clozapine on adipokine secretions/productions and lipid droplets in 3T3-L1 adipocytes, J. Pharmacol. Sci. 133 (2) (2017) 79–87.

[31] C.M. Cottingham, T. Patrick, M.A. Richards, K.D. Blackburn, Tricyclic antipsychotics promote adipogenic gene expression to potentiate preadipocyte differentiation in vitro, Hum. Cell 33 (3) (2020) 502–511.

[32] Y. Hu, E. Kutscher, G.E. Davies, Berberine inhibits SREBP-1-related clozapine and risperidone induced adipogenesis in 3T3-L1 cells, Phytother Res.: PTR 24 (12) (2010) 1831–1838.

[33] M. Fiorani, R. De Matteis, B. Canonico, G. Blandino, A. Mazzoli, M. Montanari, A. Guidarelli, O. Cantoni, Temporal correlation of morphological and biochemical changes with the recruitment of different mechanisms of reactive oxygen species formation during human SW872 cell adipogenic differentiation, Biofactors 47 (5) (2021) 837–851.

[34] S. Germani, A.C. Marchetti, A. Guidarelli, O. Cantoni, V. Sorrentino, E. Zito, Loss-of-rescue of Ryr1(I4895T)-related pathology by the genetic inhibition of the ER stress response mediator CHOP, Sci. Rep. 12 (1) (2022), 20632.

[35] E.S. Arner, A. Holmgren, Physiological functions of thioredoxin and thioredoxin reductase, Eur. J. Biochem. 267 (20) (2000) 6102–6109.

[36] Q. Cheng, E.S.J. Arner, Overexpression of recombinant selenoproteins in E. coli, Methods Mol. Biol. 1661 (2018) 231–240.

[37] G. Buffi, A. Diotallevi, M. Ceccarelli, F. Bruno, G. Castelli, F. Vitale, M. Magnani, L. Galluzzi, The host micro-RNA cfa-miR-346 is induced in canine leishmaniasis, BMC Vet. Res. 18 (1) (2022) 247.
[38] M.W. Pfaffl, A new mathematical model for relative quantification in real-time RT-PCR, Nucleic Acids Res. 29 (9) (2001) e45.
[39] M. Fiorani, A. Guidarelli, V. Capellacci, L. Cerioni, R. Crinelli, O. Cantoni, The dual role of mitochondrial superoxide in arsenite toxicity: signaling at the boundary between apoptotic commitment and cytoprotection, Toxicol. Appl. Pharmacol. 345 (2018) 26–35.
[40] E. Varone, D. Pozzer, S. Di Modica, A. Chernorudskiy, L. Nogara, M. Baraldo, M. Cinquanta, S. Fumagalli, R.N. Villar-Quiles, M.G. De Simoni, B. Blaauw, A. Ferreiro, E. Zito, SELENON (SEPN1) protects skeletal muscle from saturated fatty acid-induced ER stress and insulin resistance, Redox Biol. 24 (2019), 101176.
[41] A. Guidarelli, L. Cerioni, M. Fiorani, A. Catalani, O. Cantoni, Arsenite-induced mitochondrial superoxide formation: time and concentration requirements for the effects of the metalloid on the endoplasmic reticulum and mitochondria, J. Pharmacol. Exp. Therapeut. 373 (1) (2020) 62–71.
[42] A. Folda, A. Citta, V. Scalcon, T. Cali, F. Zonta, G. Scutari, A. Bindoli, M. P. Rigobello, Mitochondrial thioredoxin system as a modulator of cyclophilin D redox state, Sci. Rep. 6 (2016), 23071.
[43] M.E. Kauffman, M.K. Kauffman, K. Traore, H. Zhu, M.A. Trush, Z. Jia, Y.R. Li, MitoSOX-based flow cytometry for detecting mitochondrial ROS, Reactive oxygen species 2 (5) (2016) 361–370.
[44] A. Wojtala, M. Bonora, D. Malinska, P. Pinton, J. Duszynski, M.R. Wieckowski, Methods to monitor ROS production by fluorescence microscopy and fluorometry, Methods Enzymol. 542 (2014) 243–262.
[45] B. Canonico, E. Cesarini, M. Montanari, G. Di Sario, R. Campana, L. Galluzzi, F. Sola, O. Gundogdu, F. Luchetti, A. Diotallevi, W. Baffone, A. Giordano, S. Papa, Rapamycin Re-directs lysosome network, stimulates ER-remodeling, involving membrane CD317 and affecting exocytosis, in Campylobacter jejuni-lysate-infected U937 cells, Int. J. Mol. Sci. 21 (6) (2020).
[46] R.J. Baldessarini, F. Centorrino, J.G. Flood, S.A. Volpicelli, D. Huston-Lyons, B. M. Cohen, Tissue concentrations of clozapine and its metabolites in the rat, Neuropsychopharmacology: official publication of the American College of Neuropsychopharmacology 9 (2) (1993) 117–124.
[47] C. Iglesias Garcia, A. Iglesias Alonso, J. Bobes, Concentrations in plasma clozapine levels in schizophrenic and schizoaffective patients, Rev. Psiquiatía Salud Ment. 10 (4) (2017) 192–196.
[48] J. Lee, M.G. Kim, H.C. Jeong, K.H. Shin, Physiologically-based pharmacokinetic model for clozapine in Korean patients with schizophrenia, Translational and clinical pharmacology 29 (1) (2021) 33–44.
[49] G. Scaini, J. Quevedo, D. Velligan, D.L. Roberts, H. Raventos, C. Walss-Bass, Second generation antipsychotic-induced mitochondrial alterations: implications for increased risk of metabolic syndrome in patients with schizophrenia, Eur. Neuropsychopharmacol: the journal of the European College of Neuropsychopharmacology 28 (3) (2018) 369–380.
[50] A.L. Sertie, A.M. Suzuki, R.A. Sertie, S. Andreotti, F.B. Lima, M.R. Passos-Bueno, W. F. Gattaz, Effects of antipsychotics with different weight gain liabilities on human in vitro models of adipose tissue differentiation and metabolism, Progress in neuro-psychopharmacology & biological psychiatry 35 (8) (2011) 1884–1890.
[51] L. Guo, X. Li, Q.Q. Tang, Transcriptional regulation of adipocyte differentiation: a central role for CCAAT/enhancer-binding protein (C/EBP) beta, J. Biol. Chem. 290 (2) (2015) 755–761.
[52] E.D. Rosen, P. Sarraf, A.E. Troy, G. Bradwin, K. Moore, D.S. Milstone, B. M. Spiegelman, R.M. Mortensen, PPAR gamma is required for the differentiation of adipose tissue in vivo and in vitro, Mol. Cell 4 (4) (1999) 611–617.
[53] M.I. Lefterova, A.K. Haakonsson, M.A. Lazar, S. Mandrup, PPARgamma and the global map of adipogenesis and beyond, Trends Endocrinol. Metabol. 25 (6) (2014) 293–302.
[54] S.A. Belambri, V. Marzaioli, M. Hurtado-Nedelec, C. Pintard, S. Liang, Y. Liu, T. Boussetta, M.A. Gougerot-Pocidalo, R.D. Ye, P.M. Dang, J. El-Benna, Impaired p47phox phosphorylation in neutrophils from patients with p67phox-deficient chronic granulomatous disease, Blood 139 (16) (2022) 2512–2522.
[55] L.C. Pfefferkorn, P.M. Guyre, M.W. Fanger, Functional comparison of the inductions of NADPH oxidase activity and Fc gamma RI in IFN gamma-treated U937 cells, Mol. Immunol. 27 (3) (1990) 263–272.
[56] A. Guidarelli, M. Fiorani, S. Carloni, L. Cerioni, W. Balduini, O. Cantoni, The study of the mechanism of arsenite toxicity in respiration-deficient cells reveals that NADPH oxidase-derived superoxide promotes the same downstream events mediated by mitochondrial superoxide in respiration-proficient cells, Toxicol. Appl. Pharmacol. 307 (2016) 35–44.
[57] K.R. Martin, M.L. Failla, J.C. Smith, Differential susceptibility of CACO-2 and HEPG2 human cell lines to oxidative stress, J. Elisha Mitchell Sci. Soc. 113 (4) (1997) 149–162.
[58] M.S. Yang, H.W. Chan, L.C. Yu, Glutathione peroxidase and glutathione reductase activities are partially responsible for determining the susceptibility of cells to oxidative stress, Toxicology 226 (2–3) (2006) 126–130.
[59] L.E. Tebay, H. Robertson, S.T. Durant, S.R. Vitale, T.M. Penning, A.T. Dinkova-Kostova, J.D. Hayes, Mechanisms of activation of the transcription factor Nrf2 by redox stressors, nutrient cues, and energy status and the pathways through which it attenuates degenerative disease, Free Radic. Biol. Med. 88 (Pt B) (2015) 108–146.
[60] Q. Ma, Role of nrf2 in oxidative stress and toxicity, Annu. Rev. Pharmacol. Toxicol. 53 (2013) 401–426.
[61] S.C. Lu, Regulation of glutathione synthesis, Curr. Top. Cell. Regul. 36 (2000) 95–116.
[62] R. Zhao, H. Masayasu, A. Holmgren, Ebselen: a substrate for human thioredoxin reductase strongly stimulating its hydroperoxide reductase activity and a superfast thioredoxin oxidant, Proc. Natl. Acad. Sci. U.S.A. 99 (13) (2002) 8579–8584.
[63] L. Gatticchi, M. Petricciuolo, P. Scarpelli, L. Macchioni, L. Corazzi, R. Roberti, Tm7sf2 gene promotes adipocyte differentiation of mouse embryonic fibroblasts and improves insulin sensitivity, Biochim. Biophys. Acta Mol. Cell Res. 1868 (1) (2021), 118897.
[64] X. Peng, A. Giménez-Cassina, P. Petrus, M. Conrad, M. Rydén, E.S. Arnér, Thioredoxin reductase 1 suppresses adipocyte differentiation and insulin responsiveness, Sci. Rep. 6 (2016), 28080.
[65] J. Dufau, J.X. Shen, M. Couchet, T. De Castro Barbosa, N. Mejhert, L. Massier, E. Griseti, E. Mouisel, E.Z. Amri, V.M. Lauschke, M. Rydén, D. Langin, In vitro and ex vivo models of adipocytes, Am. J. Physiol. Cell Physiol. 320 (5) (2021) C822–c841.
[66] M. Al-Sayegh, H. Ali, M.H. Jamal, M. ElGindi, T. Chanyong, K. Al-Awadi, M. Abu-Farha, Mouse embryonic fibroblast adipogenic potential: a comprehensive transcriptome analysis, Adipocyte 10 (1) (2021) 1–20.
[67] K.H.T. Mau, D. Karimlou, D. Barneda, V. Brochard, C. Royer, B. Leeke, R.A. de Souza, M. Pailles, M. Percharde, S. Srinivas, A. Jouneau, M. Christian, V. Azuara, Dynamic enlargement and mobilization of lipid droplets in pluripotent cells coordinate morphogenesis during mouse peri-implantation development, Nat. Commun. 13 (1) (2022) 3861.
[68] A. Mehlem, C.E. Hagberg, L. Muhl, U. Eriksson, A. Falkevall, Imaging of neutral lipids by oil red O for analyzing the metabolic status in health and disease, Nat. Protoc. 8 (6) (2013) 1149–1154.
[69] C.E. Hagberg, Q. Li, M. Kutschke, D. Bhowmick, E. Kiss, I.G. Shabalina, M. J. Harms, O. Shilkova, V. Kozina, J. Nedergaard, J. Boucher, A. Thorell, K. L. Spalding, Flow cytometry of mouse and human adipocytes for the analysis of browning and cellular heterogeneity, Cell Rep. 24 (10) (2018) 2746–2756 e5.
[70] A. Asumendi, M.C. Morales, A. Alvarez, J. Arechaga, G. Perez-Yarza, Implication of mitochondria-derived ROS and cardiolipin peroxidation in N-(4-hydroxyphenyl) retinamide-induced apoptosis, Br. J. Cancer 86 (12) (2002) 1951–1956.
[71] K. Bedard, K.H. Krause, The NOX family of ROS-generating NADPH oxidases: physiology and pathophysiology, Physiol. Rev. 87 (1) (2007) 245–313.
[72] C. Yu, J.H. Xiao, The Keap1-Nrf2 system: a mediator between oxidative stress and aging, Oxid. Med. Cell. Longev. 2021 (2021), 6635460.
[73] H. Yuan, Y. Xu, Y. Luo, N.X. Wang, J.H. Xiao, Role of Nrf2 in cell senescence regulation, Mol. Cell. Biochem. 476 (1) (2021) 247–259.
[74] K.S. Schneider, J.Y. Chan, Emerging role of Nrf2 in adipocytes and adipose biology, Adv. Nutr. 4 (1) (2013) 62–66.
[75] X. Hu, H. Zhou, D. Zhang, S. Yang, L. Qian, H.M. Wu, P.S. Chen, B. Wilson, H. M. Gao, R.B. Lu, J.S. Hong, Clozapine protects dopaminergic neurons from inflammation-induced damage by inhibiting microglial overactivation, J. Neuroimmune Pharmacol.: the official journal of the Society on NeuroImmune Pharmacology 7 (1) (2012) 187–201.
[76] J.M. Li, A.M. Shah, Intracellular localization and preassembly of the NADPH oxidase complex in cultured endothelial cells, J. Biol. Chem. 277 (22) (2002) 19952–19960.
[77] H.T. Hsu, Y.T. Tseng, W.J. Wong, C.M. Liu, Y.C. Lo, Resveratrol prevents nanoparticles-induced inflammation and oxidative stress via downregulation of PKC-alpha and NADPH oxidase in lung epithelial A549 cells, BMC Compl. Alternative Med. 18 (1) (2018) 211.
[78] A. Jankovic, A. Korac, B. Buzadzic, V. Otasevic, A. Stancic, A. Daiber, B. Korac, Redox implications in adipose tissue (dys)function–A new look at old acquaintances, Redox Biol. 6 (2015) 19–32.
[79] K.E. Wellen, C.B. Thompson, Cellular metabolic stress: considering how cells respond to nutrient excess, Mol. Cell 40 (2) (2010) 323–332.
[80] A.T. Dinkova-Kostova, A.Y. Abramov, The emerging role of Nrf2 in mitochondrial function, Free Radic. Biol. Med. 88 (Pt B) (2015) 179–188.
[81] S. Heinonen, R. Jokinen, A. Rissanen, K.H. Pietiläinen, White adipose tissue mitochondrial metabolism in health and in obesity, Obes. Rev. 21 (2020), e12958.
[82] J.S. Bhatti, G.K. Bhatti, P.H. Reddy, Mitochondrial dysfunction and oxidative stress in metabolic disorders— a step towards mitochondria based therapeutic strategies, Biochim. Biophys. Acta 1863 (2017) 1066–1077.
[83] J.A. Sipkens, N. Hahn, C.S. van den Brand, C. Meischl, S.A. Cillessen, D.E. Smith, L. J. Juffermans, R.J. Musters, D. Roos, C. Jakobs, H.J. Blom, Y.M. Smulders, P. A. Krijnen, C.D. Stehouwer, J.A. Rauwerda, V.W. van Hinsbergh, H.W. Niessen, Homocysteine-induced apoptosis in endothelial cells coincides with nuclear NOX2 and peri-nuclear NOX4 activity, Cell Biochem. Biophys. 67 (2) (2013) 341–352.